SOVIET PHYSICS

USPEKHI

A Translation of Uspekhi Fizicheskikh Nauk

É. V. Shpol'skiĭ (Editor in Chief), S. G. Suvorov (Associate Editor),
D. I. Blokhintsev, V. L. Ginzburg, B. B. Kadomtsev, L. D. Keldysh,
S. T. Konobeevskiĭ, F. L. Shapiro, V. A. Ugarov, V. I. Veksler,
Ya. B. Zel'dovich (Editorial Board).

SOVIET PHYSICS USPEKHI (Russian Vol. 99, Nos. 3 and 4) MAY-JUNE 1970

538.89

CONTINUOUSLY OPERATING ARGON ION LASERS

V. F. KITAEVA, A. N. ODINTSOV, and N. N. SOBOLEV

P. N. Lebedev Physics Institute, USSR Academy of Sciences; Moscow State University

Usp. Fiz. Nauk 99, 361–416 (November, 1969)

I. INTRODUCTION

THE first gas-discharge laser was developed by A. Javan, W. Bennett, and D. Herriott in 1961[1]. This was the first continuous laser using a mixture of helium and neon. The publication of[1] was followed by a flood of research, the results of which was the discovery of a large number of gas systems and transitions that made possible generation in a wide range of the spectrum, from the ultraviolet to the far infrared. A summary of this research is given in a number of reviews[2-5].

The present status of gas laser development is characterized by a sharp decrease in the volume of basic research and by a concentration of efforts on the study of the operating mechanism, improvements, and applications of some of the most outstanding and promising representatives of the large family of gas-discharge lasers. These are: 1) the helium-neon laser, operating on atomic transitions at 0.63, 1.15, and 3.39 μ; 2) lasers using noble-gas ions and generating on a large number of lines in yellow and blue-green regions of the spectrum; 3) molecular CO_2 laser, generating on rotational-vibrational transitions in the 9.4–10.6 μ region.

The most widely used in physics laboratories, and at the same time the most thoroughly investigated and technologically developed, is the He-Ne laser[6,7]. However, the radiation output power and the efficiency of this type of laser are low.

The largest output power (~10 kW) of continuous laser emission and the highest efficiency (~0.1) is possessed by the CO_2 laser, but its radiation lies in the infrared region of the spectrum. Results of investigations devoted to this type of laser, formed through May 1966, are summarized in[8-11].

In the visible region of the spectrum, the largest continuous radiation power (~100 W) and the highest efficiency (~10^{-3}) were obtained with an argon-ion laser (Ar^+ laser). These qualities, and particularly the fact that its radiation lies in the blue-green region of the spectrum, for which the most sensitive receivers are available, points to great prospects for the use of Ar^+ lasers for such important applications as holography[12], color television[13], underwater television and radar, production of color[14] and three-dimensional motion pictures, recording and reading of information with magnetic film[15], variation of resistances in microcircuits[16], space flights[17], physical investigations in the field of nonlinear optics and light scattering[18], research in biology[19], medicine, etc.

Naturally, a large number of papers have been devoted to this type of laser, some of which have been considered in the already cited reviews[4,5] and in the articles of W. Bridges and A. Chester on ion lasers[20]. The first review devoted especially to Ar^+ lasers was written in 1966 by R. Paananen[17a], and the second in 1967 by P. Armand[17b].

The present review summarizes the research and development performed in the last three years on continuous Ar^+ lasers, including papers reported in May 1968 at the International Conference on Quantum Electronics in Miami. In the historical review (Ch. II) we consider the main stages of the development of research during the period from 1964 through 1965 inclusive, when the basic trends of development and research of Ar^+ lasers were established. In Ch. III we describe the results of developments of different types of continuous Ar^+ lasers, their features, and the influence of different parameters on the output power of laser emission.

The next four chapters are devoted to the physical picture of the occurrence of inversion in Ar^+ lasers. In Ch. IV we discuss the hypotheses concerning the mechanism of formation of inverted population in Ar^+ lasers, first advanced by Bennett and co-workers[21] and by E. Gordon and co-workers[22], as well as their modifications. Chapter V contains the results of investigations of the properties of the plasma of the Ar^+ laser, while Ch. VI gives the theoretical values of the probabilities of the radiative transitions and the rates of electronic excitation of argon ions. In Ch. VII is given the calculation of the rate of pumping and inverted population in Ar^+ lasers and a comparison of

Copyright © by American Institute of Physics 1970

calculation with experiment.

There is only a limited number of papers dealing with the spectral composition of the generation of Ar^+ lasers, with methods of mode selection, and with methods of frequency stabilization. However, taking into account the importance of these problems, we have decided to include in the present review a chapter devoted to the investigations of the frequency spectrum of longitudinal modes (Ch. VIII) and to single-frequency Ar^+ lasers (Ch. IX). We have also included Ch. X, devoted to problems connected with the efficiency of utilization of the active medium and the generation power in single-frequency and multifrequency regimes.

II. HISTORICAL OUTLINE

The generation of coherent radiation on the lines of the argon ion, which lie in the blue-green region of the spectrum, was first realized in a pulsed regime in 1964, almost simultaneously by Bridges[23] and by G. Convert et al.[24]. This discovery was made accidentally, using argon as a buffer gas in a mercury discharge[25], which in turn was used to study generation on the ion lines of mercury. Bridges[23] observed generation on the ten lines of Ar II indicated in Fig. 1, while Convert et al. observed generation on eight lines. As seen from the figure, generation occurs on transitions between the levels of 4s and 4p configurations of Ar II. R. McFarlane[26] obtained generation on three Ar III lines located in the ultraviolet region of the spectrum. H. Heard and J. Peterson[27] investigated a mixture of mercury and argon and observed generation of Ar II lines not only for short pulses (~5 μsec), but also long ones (~100–200 μsec). It was established that the output power on the λ 4765 Å line follows the current in time and the λ 4880 Å line generates in the afterglow. Bennett and co-workers[21] also investigated pulse generation of the Ar II lines for short (~20 nsec) and long (~1 msec) pulses (see also[7]).

It was reported already in these first papers that the gain for the λ4880, 5145, and 4765 Å lines amounts to ~200% per meter of discharge length, and the output power in the pulse for each of the λ4880, 5145, 4765 Å lines is of the order of 10 W. At the present time, the radiation power in the pulse reaches several times ten kW.

Continuous generation on Ar II lines was first observed by E. Gordon, E. Labuda, and W. Bridges[22], who used gas-discharge tubes with diameters from 1.2 to 2.5 mm and currents up to 15 A at an argon pressure on the order of several tenths of a Torr. A power up to 80 mW was obtained, but the effect of transfer of the gas[28], observed at large current densities, made it impossible to obtain stationary generation. To estimate this effect, Gordon and Labuda[29] proposed to use a bypass channel parallel to the gas-discharge tube.

In August 1964 there was published a communication[30] by the Raytheon Company reporting development of a continuous Ar^+ laser with a power exceeding 1 W, this being accomplished as a result of placing rodlike magnets around the discharge tube. In December 1964, the same firm reported[31] attainment of a generation power of ~7 W on the Ar II lines and of an efficiency ~0.053%, and the development of an Ar^+ laser with an output power up to 15 W.

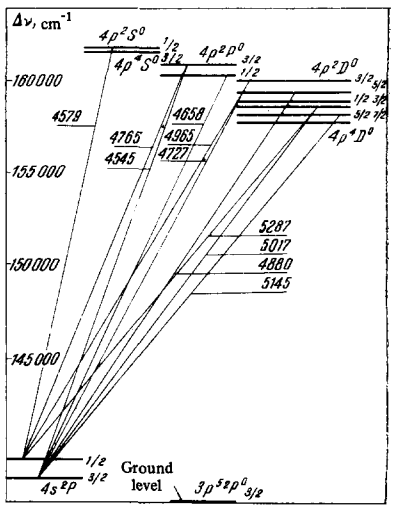

FIG. 1. Part of the level scheme of Ar II: the principal lines of generation of continuous argon ion lasers.

The first sufficiently detailed investigation of the dependence of the output power of an Ar^+ laser on different parameters was that by Gordon and co-workers[32]. It was established that the generation power increases with increasing current and that further increase of the power is limited by the destruction of the capillary as a result of ion bombardment and heating of the walls by the energy released in the gas discharge. Damage in a capillary of diameter 2.5 mm at a wall thickness ~1 mm, cooled with running water, sets in at currents ~ 30 A. The use of ceramic capillaries for Ar^+ lasers has made it possible to work with higher current densities than with quartz capillaries.

A considerable increase in the power of Ar^+ lasers was obtained by applying an external longitudinal magnetic field. Experiments have shown that a suitably chosen longitudinal magnetic field not only increases the generated power at a given current, but, most importantly, makes it possible to increase the maximum current density that can be carried by a given capillary. According to[32], for a tube of 2.5 mm diameter at a discharge current ~30 A, the maximum per-unit power increases from 1 W/cm^3 without a magnetic field to ~2.8 W/cm^3 at the optimal magnetic field. It was also noted in[32] that in lasers with longitudinal magnetic fields the presence of windows inclined at the Brewster angle decreases the power loss connected with circular polarization of the components in the case of Zeeman splitting in a longitudinal magnetic field. When a magnetic field is used, it is advantageous to employ high-transmission output windows placed perpendicular to the discharge axis.

The insufficient thermal conductivity of quartz, which limits the useful power needed to increase the generation power, has suggested the replacement of the quartz capillary with a set of metallic discs with apertures bounding the discharge, separated by quartz rings[33,34]. In such a sectionalized tube the resistance to ion bombardment and the thermal conductivity are much higher. The increased heat dissipation makes it possible to increase appreciably the useful power, and

consequently also the generation power. The first experiments performed with such tubes at metallic-disc aperture diameters of 1 and 2 mm have made it possible to obtain, without a magnetic field, powers of 0.25 and 1 W respectively and a per-unit power of ~ 1 W/cm^3[34].

In October 1965, W. Bell published a paper[35] in which he proposed to feed an Ar^+ laser with a high-frequency pulsed discharge. The closed discharge tube is in this case a secondary "winding" of a radio-frequency transformer. In a tube 60 cm long and 5 mm in diameter, at a 1% off-duty cycle of the pulses, an average power of ~ 0.25 W was obtained on the Ar II line[36]. Generation was also observed in the ultraviolet region (3300–3600 Å) on the lines of Ar II, Ar III, and Kr III. A longitudinal magnetic field greatly increased the power in this discharge (by a factor of 10). Bell's work was the basis for further suggestions of realization of Ar^+ lasers of continuous action with radio-frequency supply.

The first hypotheses concerning the mechanisms that produce population inversion in Ar^+ lasers were advanced by Bennett and co-workers[21] and by Gordon and co-workers[22]. According to Bennett's hypothesis, pumping at the upper laser levels of Ar II, belonging to the 4p configuration, is the result of the two-electron process $Ar + e \rightarrow (Ar^+)^* + 2e$, i.e., as a result of simultaneous detachment of an electron from the argon atom and excitation of the argon ion. In Gordon's opinion, the excitation of the upper Ar II laser levels occurs in two stages:

$$Ar + e \rightarrow Ar^+ + 2e, \quad Ar^+ + e \rightarrow (Ar^+)^* + e,$$

i.e., the excitation of the levels of the 4p configuration occurs possibly from the ground state of the ions.

These two hypotheses were followed by a number of others concerning the population of the levels of Ar II of the 4p configuration from metastable states of the atom or ion Ar II[4], and also concerning the population of the upper laser levels from higher lying levels. The question of which of these hypotheses corresponds to reality can obviously be answered only by means of detailed data on the properties of the plasma and on the probabilities of the radiative and electronic processes. Fundamental work was performed by H. Statz et al.[37], who calculated the radiative probabilities of many transitions of Ar II which have a bearing on generation. They reached the conclusion that the main cause of the destruction of the lower laser levels of Ar II (the configuration 4s) should be radiative processes. However, the question of the role played by the electronic processes in the destruction and creation of laser-level population can again not be answered without additional experimental and theoretical investigations. This briefly was the status of the problem concerning argon ion lasers at the beginning of 1966.

III. CONSTRUCTION AND FEATURES OF CONTINUOUS Ar^+ LASERS. FUNDAMENTAL EXPERIMENTAL RESULTS

As a result of investigations performed in 1964–1965, three basic types of continuous Ar^+ lasers, fed with direct current, have been developed: 1) quartz, 2) ceramic, and 3) sectionalized. Bell's researches[35], mentioned at the end of Ch. II, have led to the development of a continuous Ar^+ laser with a radio-frequency supply. These types of Ar^+ lasers will be studied in greater detail later on. We shall also consider the influence of the discharge parameters and of an external axial magnetic field on the output power of Ar^+ lasers, as well as the role of the transfer of the gas.

Generation on lines of inert-gas ions is observed at high current densities, on the order of several hundred A/cm^2, in low-pressure discharges. High current densities are needed to maintain a sufficiently high degree of ionization of the gas and a high electron temperature. The main requirements imposed on the construction of the tube therefore reduce to the following. The tube walls must withstand high thermal loads (hundreds of W/cm^2) and ion bombardment. The electrodes must be designed for discharge currents up to several hundred amperes and have high endurance to electron and ion bombardment. To equalize the pressure in the anode and cathode tubes during the discharge process it is necessary to use an additional bypass channel. A schematic diagram of the construction of a continuous-radiation Ar^+ laser is shown in Fig. 2. The capillary is usually cooled with water. The bypass channel is constructed either in the form of a tube sealed into the anode and cathode tubes parallel to the capillary and placed either inside or outside the water-cooling jacket, or else in the form of an additional sheath located on top of the water-cooling jacket. The anode is cooled with water and usually has the form of a metallic cylinder with double walls or the form of a cylindrical helix. Oxide cathodes of various designs are extensively used. Recently, impregnated cathodes have come into use, in the form of a porous tungsten sponges impregnated with barium and calcium aluminate. These cathodes have a larger emissivity. When working with currents on the order of hundreds of amperes, the dimensions of these cathodes are smaller by a factor of several times ten than the dimensions of oxide cathodes. They do not lose their emissivity after multiple breaking of the vacuum in the tube.

The cathode used in[98] was hollow and cooled with water. The authors state that such a cathode makes it possible, in principle, to operate with arbitrary currents; however, the cathode used by them began to

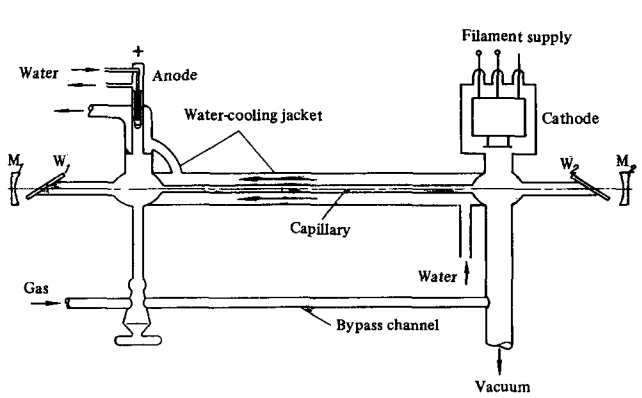

FIG. 2. Diagram of continuous Ar^+ laser, W_1, W_2 – windows placed at the Brewster angle; M_1, M_2 – mirrors.

"sputter" at discharge currents on the order of 30–40 A, leading to a decrease in the output power. The use of a hollow cathode is reported also in[39].

The material most frequently used for the main part of the capillary of the Ar^+ laser is quartz.

1. Laser with Quartz Capillary

Quartz is one of the most suitable materials for discharge tubes. The high heat endurance, the good electric insulating properties, and the endurance to erosion are the properties responsible for the extensive use of quartz in ionic argon lasers. There are no technical difficulties in the preparation of quartz discharge tubes of different diameters and lengths. This apparently explains why most experimental investigations reported below were made with lasers having glass capillaries.

The discharge-tube diameter used by various authors ranges from 1 to 15–20 mm, and the tube length runs from 10 cm to several meters. The basic information concerning the radiation power obtained with continuous Ar^+ lasers with tubes of various lengths and various diameters is contained in[30,31,34,38,40-57].

In the Soviet Union, the first sealed one-watt continuous Ar^+ laser was constructed in 1965 and was exhibited at the National Economy Fair under the title "Klen." The instrument was improved in 1966 and demonstrated in 1967 at the Montreal Exposition under the tital "Malakhit." In 1966 there was developed in the USSR one more type of one-watt argon laser, LG-106, intended for commercial manufacture. An overall view of Lg-106 is shown in Fig. 3. Both "Malakhit" and LG-106 are sealed instruments with quartz capillaries. The discharge is in a longitudinal magnetic field. The power supplies are compact. A dismountable quartz Ar^+ laser was also developed[58]. The possibility of easily replacing the individual units is undoubtedly an advantage of the dismountable construction of the laser.

The largest generation power (53 W) was obtained under laboratory conditions[46] with a quartz tube 260 cm long of 7.75 mm inside diameter and with an external longitudinal magnetic field of ~1000 Oe, at a discharge current of 100 A; another laser was obtained in[47a] and was rated 100 W, using a tube of 10 mm diameter at a discharge current ~ 300 A. It must be noted that the large radiation power of the Ar^+ laser was obtained in[47a] without an external magnetic field, i.e., without additional energy consumption. The power supply of the tube was also simple—it could be fed from either an ac line or a dc line. The authors of that paper believe that the power obtained by them is not the ultimate one, and a power of 0.5 kW is perfectly realistic.*

2. Lasers with Ceramic Capillaries

In addition to having a large number of advantages, quartz also has a major shortcoming—low thermal conductivity. The insufficient thermal conductivity of the quartz limits the power consumed, and consequently also the output power of the continuous Ar^+ laser. Investigations were performed to ascertain the feasibility of using discharge tubes of various ceramics and anodized aluminum.

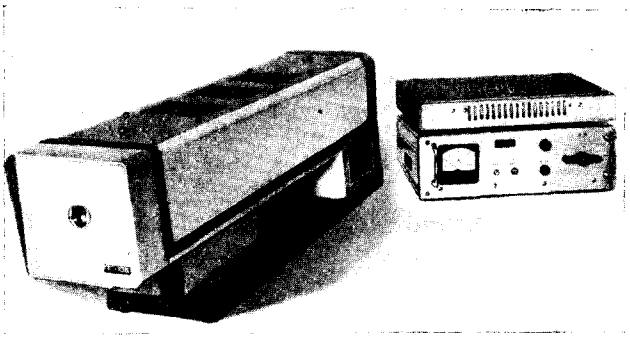

FIG. 3. Overall view of ionic argon laser LG-106 and the power supply BP-27. Output voltage 510 V; load current 15 A; fed from 380 – 220 V, 50 Hz line.

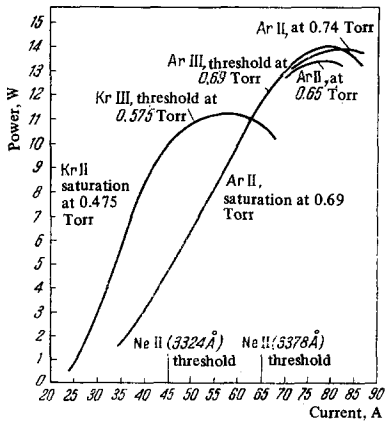

FIG. 4. Radiation power vs. discharge current for Ar II, Ar III, Kr II, and Kr III [51] (capillary diameter 3.5 mm).

Ar^+ lasers with capillaries of ceramic yielded a power of 1 W at a service life to 300 hours[48], and later 5 W[50] at a service life of 1000 hours. Under the same conditions, the service life of a ceramic capillary was 1000 hours, and that of a quartz capillary 100 hours.[59]

In[51] is described a laser using ceramic tubes (the length of each tube is 2.7 cm, the number of tubes is 26), built into an aluminum anodized tube, thus ensuring mechanical strength and cooling of the ceramic inserts. At a capillary diameter 3.5 mm and with an external magnetic longitudinal field applied, it turned out to be possible to operate with currents up to 90 A in a tube of this construction. Consequently, current saturation of the generation power was attained for the first time in a continuous Ar^+ laser (Fig. 4).

As seen from Fig. 4, at a current of 75 A and a pressure of 0.65–0.74 Torr, the generation power reaches a maximum of 14.1 W, corresponding to a generation power density 2.5 W/cm^3. With further increase of the current, the generation power decreases. With a laser of this construction, the author succeeded also in obtaining for the first time continuous generation using doubly-ionized Ar and Kr in the ultraviolet

*See also pp. 726-727.

region (Ar III, λ 3511 Å; Kr III, λ 3507 Å) of the spectrum. The radiation power on the Ar III λ 3511 Å line was 13 mW at a total radiation power of the Ar II lines of 14.1 W.

The largest radiation power in the ultraviolet regime was obtained in[47b], namely 1.5 W on the λ 3511 and 3668 Å lines of Ar III.

It was also proposed[60] to use tubes made of anodized aluminum in continuous Ar^+ lasers. Experiments were performed with a tube 30 cm long and 2.9 mm in diameter. The film thickness was 60–100 μ. At an average current of 10 A and a maximum current of 19 A, the tube operated for 50 hours without noticeable wear. At a current of 18 A, the power obtained was 136 mW at a pressure of 0.35 Torr. The authors believe that such a tube can withstand current up to 60 A and ensure a radiation power of several watts.

3. Sectionalized Lasers

Great success was accomplished with sectionalized tubes, on the basis of which most commercial Ar^+ lasers are now constructed. It was possible to increase greatly the consumed power, and by the same token also the output-radiation power, by using tubes made up of metallic washers. Such a tube is shown schematically in Fig. 5a. The metallic washers are separated by quartz rings. In[38] they proposed a tube design (Fig. 5b) using metallic washers separated by rubber liners. The cathode was of the hollow type.

A generation power of 0.25 W at a current of 10 A was obtained[42] in the tube assembled from molybdenum discs, at a capillary length of 25 cm and a diameter of 1 mm.

A power of 1 W was obtained in a tube having the same capillary length and a diameter of 2 mm at a current of 40 A. The per-unit radiation power of these tubes was 1 W/cm³.

It is noted in[52] that the main shortcoming of tubes of such a construction is the sputtering of the metal, which leads to erosion of the electrodes and to aging. The authors of the cited paper experimented with tubes made up of Mo, Ta, and graphite washers. The experiments have shown that the best material is graphite. The construction of this tube is shown in Fig. 5c. Investigations were made to determine the service life. For tubes with a capillary length 15 cm, a diameter 2 mm, and a current of 9 A (impregnated cathode), the output power obtained was 80–100 mW at an external magnetic field of 800 Oe. After 1000 hours of operation, no changes were observed in the output power on the surface of graphite washers. With a tube 60 cm long and 4 mm in diameter, made of graphite washers, an output power of 10 W was obtained at a service life more than 100 hours. Commercial samples of sectionalized lasers of graphite[53,56] are being produced rated up to 2 W with a service life of 1000 hours and ~10 W with a service life of ~100 hours.

Using a sectionalized tube of graphite washers, Fendley (see[52]) observed generation in a number of Ar III lines[17]. The capillary diameter in these experiments was 0.7 mm, the length of the discharge part was 35 cm. At a current of 25 A, an optimal magnetic field of 1200 Oe, and an argon pressure 0.34 Torr,

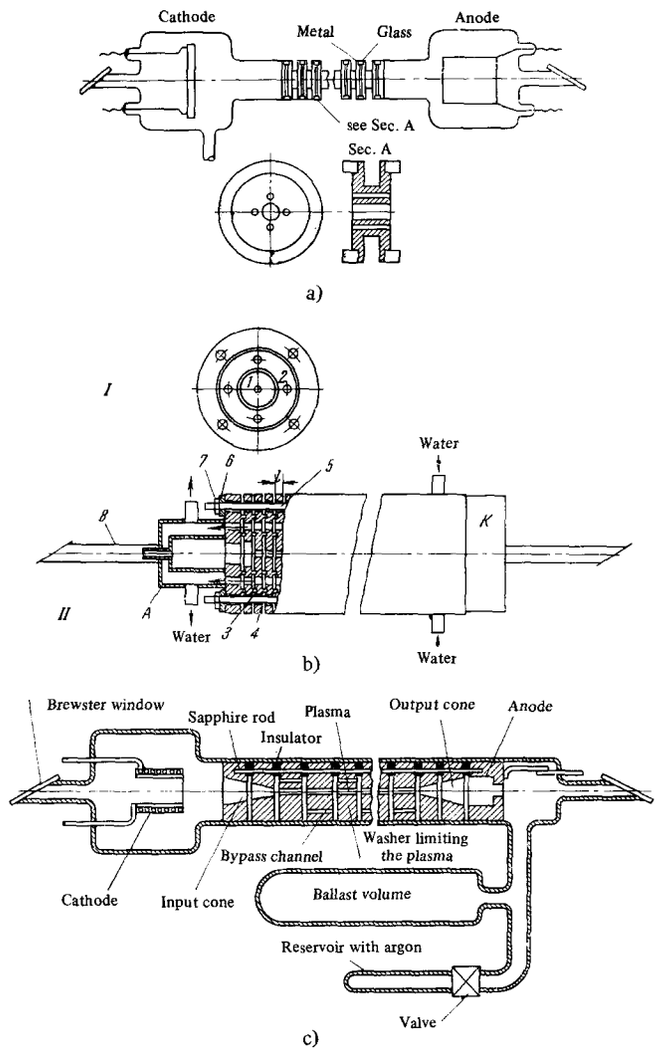

FIG. 5. Tubes: a) for an Ar^+ laser with a sectionalized capillary [33]; b) sectionalized with hollow cathodes [38]; c) for an Ar^+ laser with a capillary of graphite washers [52]. In b I: 1 – working aperture 2.5 mm diameter, 2 – aperture for water; in b II: A – anode, K – cathode, 3 – rubber liner, 4 – washer, 5 – tightening bolts with insulation, 6 – insulating ring, 7 – lock nuts, 8 – glass tube with water cooling. The active length of the section was 17.5 cm.

the following gain coefficients were obtained for the Ar III lines: λ 3638 Å–0.21 m^{-1}, 3511 Å–0.21 m^{-1}, 3336 Å–0.1 m^{-1}. In both ends of the tube, a radiation power of 68 mW and 60 mW was obtained in the λ 3638 Å and 3511 A lines, respectively. For all three lines of Ar III, the total radiation power was ~140 mW. Commercial argon ion lasers are being produced with quartz, ceramic, and sectionalized capillaries. Lasers with quartz capillaries give an output power from several hundred mW to ~ 1 W (individual units up to ~5 W), while lasers with ceramic and sectionalized capillaries that produce 3–10 W and have a much larger service life.

Recently, sectionalized Ar^+ lasers made of BeO ceramic have become available[56b]. These lasers have a service life of ~1000 hours at a radiation power up to 7 W.

4. Laser with Radio-frequency Supply and Laser Operating at Cyclotron Resonance

The argon ion laser with radio-frequency supply[35] is of interest primarily because there are no electrodes in the discharge tube. This makes it possible to work with active gases (laser action on selenium, arsenic, and bromine ions was first obtained in such a discharge).

Among the favorable properties of such excitation is also the decreased erosion of the quartz capillary, the absence of electrophoresis and aging, the absence of noise in the radiation, narrower atomic lines (approximately 30% narrower than in a dc discharge). The construction of an Ar^+ laser with radio-frequency pulsed supply, proposed by Bell, is shown in Fig. 6.

Different configurations of inductive coupling between the laser and the primary winding of the radio frequency transformer have been investigated[61], and experiments aimed at determining the parameter of such a discharge have been performed.

In[62], the tube was fed continuously from a radio-frequency generator with the aid of a loop located at a fixed position relative to the tube (Fig. 7). The total maximum output power for five lines was 1.4 W at a power supply of 1400 W. The length of the capillary was 10 to 40 cm, and the diameter 1 to 2.8 mm. It turns out that the voltage drop on the tube is independent of the gas pressure, of the current, and of the frequency in the 3.5–2.8 MHz region, and depends on the tube diameter. The axial magnetic field decreases the voltage drop on the tube and increases the output power of the laser. The authors assume that it is perfectly feasible to obtain with Ar II a power of ~10 W at an efficiency of 0.2%. On the basis of Bell's investigations, the firm Spectra Physics has developed a single-mode Ar^+ laser with inductive excitation[63] and with an output-power of ~2 W. Figure 8 shows a diagram of this laser. The output-power distribution among the generation lines is shown in Table I. The width of the beam is 1.2 mm and the divergence 0.7 mrad. The guaranteed service life is 1000 hours.

Quasicontinuous generation on λ 4880 Å in a tube of 15 cm length and 10 mm diameter was obtained in[64] using inductive excitation of the plasma. The tube was placed in a secondary winding of a transformer, the primary winding of which was fed from a square-wave generator at a frequency of 2.5 kHz. The output power was 150 mW.

An original Ar^+ laser construction is described in[65]. It is proposed to produce the population inversion by direct excitation of the upper level from the ground state of the argon atom. To obtain electrons of energy ~35 eV, which are needed for the realization of this process, it is proposed to use crossed electric and magnetic fields. An electron situated in a magnetic field and in a perpendicular alternating electric field of the cyclotron frequency will move along a helix and can acquire energy from the electric field in a large number of cycles. The proposed laser design is illustrated in Fig. 9. An electric field parallel to the tube axis was produced by a magnetron of 1 kW power, and a perpendicular magnetic field was produced by an electromagnet along 10 cm of the tube length (diameter 3 mm). Generation was observed on five lines. In view of the fact that at a power input ~500 W the total output power was 5 mW, this type of laser can hardly be of practical interest.

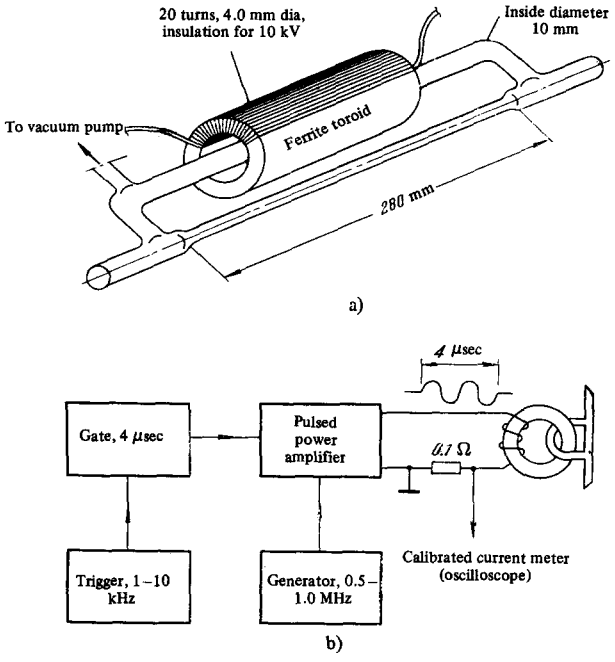

FIG. 6. Ar^+ laser with radio-frequency pulsed supply [35]. a) Tube with excitation coil (capillary with 4.0 mm diameter); b) block diagram of supply.

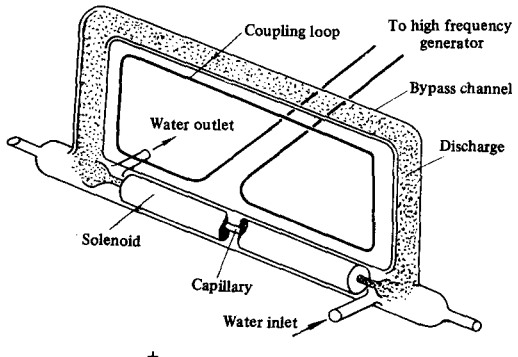

FIG. 7. Ar^+ laser with radio-frequency supply.

Table I

λ, Å	Power, mW	λ, Å	Power, mW
4880	900	4579	25
5145	900	5017	25
4965	60	4727	15
4765	60	4658	15

5. Principal Experimental Results

The first experiments on Ar^+ lasers were performed with discharge tubes of small diameter (1.25–4 mm). It was established that the properties of the discharge used for argon ionic lasers are quite

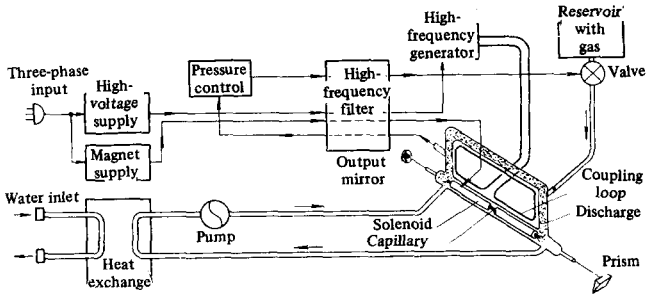

FIG. 8. Diagram of "Spectra Physics" Ar^+ laser with induction excitation [63], with output power ~ 2 W.

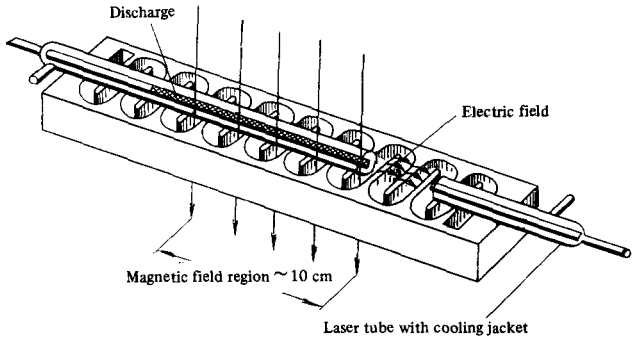

FIG. 9. Construction of Ar^+ laser operating on cyclotron resonance [65].

peculiar. Only at small current densities, close to the generation threshold, was there a downward sloping discharge characteristic. For most regimes, when the generation power was relatively large, the discharge characteristics sloped upward. It can therefore be assumed approximately that the field intensity E does not depend on the current. In addition, in the region of pressure characteristic of the operation of the Ar^+ laser, the field intensity does not depend, or more accurately speaking, depends little, on the pressure. To the contrary, the dependence of E on the tube diameter D is quite strong, and according to measurements performed at the Bell Telephone Laboratories[66].

$$E = 1.23D^{-1}\ (\text{V/cm}), \qquad (1)$$

If D is in centimeters.

The dependence of the output power on the discharge current was first obtained in[22] for a tube of 1.9 mm diameter at current densities 15–300 A/cm². It turns out that at a sufficiently large distance from the threshold the output power increases in proportion to the square of the current. The saturation of the power as a function of the current cannot be observed in a quartz tube, since the capillary is destroyed by large currents.

The smallest value of the threshold current (i = 0.37 A at l = 10 cm and D = 1.25 mm) is possessed by the λ 4880 Å line of Ar II ($4s^2P_{3/2}$–$4p^2D_{5/2}$). With increasing current, following λ 4880 Å at 1.5 and 1.85 A respectively, there begins generation on λ 4765 Å ($4s^2P_{1/2}$–$4p^2P_{3/2}$) and 5145 Å ($4s^2P_{3/2}$–$4p^4D_{5/2}$). Far from the generation threshold, the main coherent radiation power (~70–80%) of the Ar^+ laser is contained in the λ 4880 and 5145 Å lines. It can be

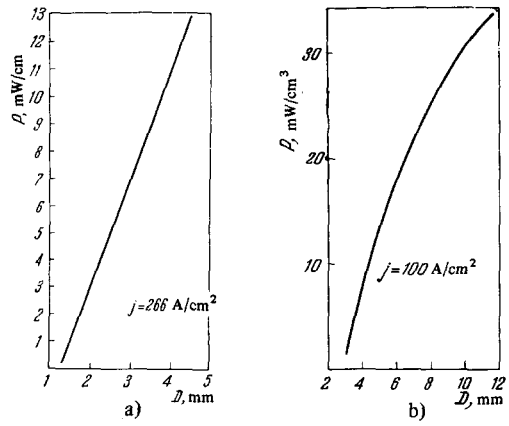

FIG. 10. a) Dependence of the output power from a unit length of the discharge on the diameter of the capillary; b) dependence of the output power from a unit volume of the discharge on the diameter of the capillary.

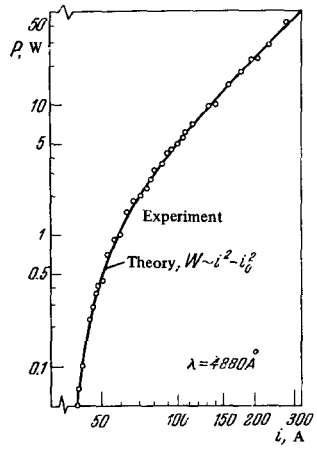

FIG. 11

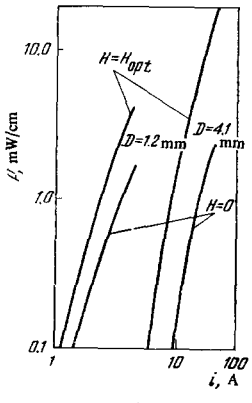

FIG. 12

FIG. 11. Dependence of the laser radiation power on the discharge current [47].

FIG. 12. Dependence of the output power per unit discharge length on the discharge current for capillaries of 1.2 and 4.1 mm diameter at $H = H_{opt}$ and H = 0 [32].

divided approximately equally between them if the transmission curves of the mirrors are suitably chosen.

At a fixed discharge current, the generation power depends strongly on the pressure of the argon filling the capillary. For each value of the current, there is an optimal pressure. With increasing current, the optimal pressure increases. As will be shown below, this is due to the increase of the rate at which the gas is forced out from the capillary into the colder parts of the discharge tube. The range of working pressure of a continuous-action Ar^+ laser is ~0.3–0.6 Torr (for capillaries of 2–4 mm diameter without an external magnetic field).

As was already indicated above, the first studies of continuous Ar^+ lasers were performed with small-diameter discharge tubes. The use of large cross section discharge tubes for lasers was hindered for some time by the lack of cathodes suitable for work at large

currents (~100 A) not in vacuum but in an argon atmosphere. At the present time these difficulties have been overcome, and experiments with discharge tubes of large cross sections have shown that the power both per unit length and per unit volume (at j = const) increases with increasing diameter of the discharge tube (Figs. 10a and b; the plots are based on the data of of[34,17]).

Particular success in this direction was attained by the authors of[47a]. As indicated above, by using a quartz discharge tube of 10 mm diameter they obtained a generation power of ~100 W. Investigations of lasers with discharge tubes of 15 mm diameter, reported in that reference, have shown that formula (1) is valid in practice also for tubes of large diameter (the numerical coefficients differ in[66] and[47] by 7%). The optimal pressure, as a function of the diameter of the tube D, is determined at jD < 100 A/cm by the relation

$$p_0^* = 0.05 D^{-1} \text{ (Torr)}, \qquad (2)$$

where D is in centimeters. The authors of[47a] have also found that the efficiency in a tube of 7–15 mm diameter is proportional to the tube diameter, and far from the threshold the power, just as in small-diameter tubes, increases in proportion to the square of the current (Fig. 11). As seen from Fig. 11, the experimental points fit satisfactorily a quadratic dependence on the current in the range from 40 to 400 A/cm^2.

a) Superposition of an external magnetic field on the discharge of an ion laser leads to an appreciable increase of the generation power. This is first observed by Gordon et al.[32], who placed an argon ion laser in a longitudinal magnetic field in order to decrease the ion bombardment and the thermal mode on the quartz, and by the same token increase the service life to the laser.

The dependence of the power on the field turned out to be nonmonotonic, and the power depends on the diameter of the capillary (the investigations were performed with capillaries of 1–8 mm diameter). For each capillary diameter there is a definite optimal magnetic field, yielding a maximum increase of the output power. This optimal field is the smaller, the larger the diameter of the capillary. The increase of the output power upon superposition of a magnetic field is shown in Fig. 12, for two capillary diameters (1.2 and 4.1 mm). At currents greatly exceeding the threshold values, the ratio of the increase of the output power when the optimal magnetic field is applied, for the capillaries with 1.2 and 4.1 mm diameter, is almost proportional to the ratio of the diameters. The ratio of the increases of the power with the field applied is 2.9 for these tubes, whereas the ratio of the diameters is 3.3.

The value of the optimal magnetic field H_{opt} depends on the discharge and on the gas pressure. With increasing current and pressure, H_{opt} decreases. Figure 13 illustrates the dependence of H_{opt} and of the corresponding generation powers on the gas pressure for a capillary of 4 mm diameter, 28 cm length, at a current 30 A[42]. As seen from the figure, when p increases from 0.5 to 0.9 Torr, H_{opt} decreases

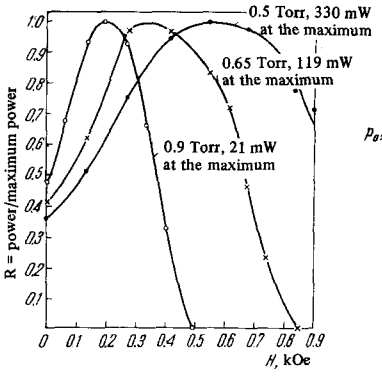

FIG. 13

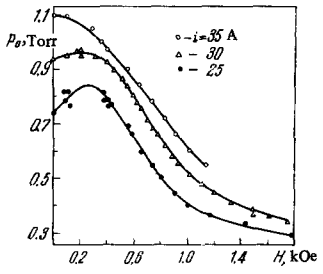

FIG. 14

FIG. 13. Dependence of relative generation power R on the external magnetic field for different filling pressures [42].

FIG. 14. Threshold power curves corresponding to the instant of cessation of generation on the discharge axis [42].

from 600 to 200 Oe. The threshold generation curve shown in Fig. 14 separate the region of values of p and H at which the generation is impossible (above the curve), from the region of these values of p and H at which generation is possible. Investigations of the distribution of the generation power over the cross section of the beam have shown that the decrease of the generation power with increasing p and H (after reaching the optimal values P_{opt} and H_{opt}), is connected with the cessation of the generation on the discharge axis and subsequent expansion of this region up to the walls of the discharge tube. When $p > p_{opt}$ and $H > H_{opt}$, the generation occurs already not in the entire cross section of the discharge tube, but only in a region located at a certain distance from the tube axis. Similar laser rings were observed also with pulsed lasers[67] and were attributed to dragging of the resonant radiation[68].

Detailed investigations of the dependence of the output power on the principal discharge parameters namely current, gas pressure, axial magnetic field, and also on the diameter and length of the capillary for lasers with quartz capillaries and with a radiation power of several watts, are reported in[69]. The main result of that paper is shown in Table II, which gives an idea of the optimal parameters of the discharge for tubes of varying diameter. It is seen from the table that a change from a tube of 3 mm diameter to a tube of 4 mm diameter leads to an appreciable increase of the radiation power and of the efficiency of Ar^+ lasers (it was impossible to carry out the comparison with a tube of 6 mm diameter, for in this case the mirrors were not optimal).

It should be noted that an external magnetic field increases the output power not only of a continuously acting Ar^+ laser, but also of a pulsed laser. The effect here, however, is much weaker. As was established in[70], when a magnetic field is superimposed, the generation power of a pulsed laser increases, depending on the discharge conditions, by 20–100%. The efficiency of the pulsed laser increases by approximately the same amount.

b) Transfer of gas, due to the appearance of elec-

Table II

Output power, W	p_0, Torr	H, Oe	i, A	j, A/cm^2	Voltage drop across tube, V, volts	Power fed to tube, W	Efficiency, in un. of 10^{-4}
Tube dia. 3 mm, l = 46 cm							
3.30	0.95	1260	27.5	389	180	4950	6.67
2.19	0.72	1260	22.5	318	168	3780	5.79
1.48	0.50	1000	17.5	248	159	2780	5.32
0.99	0.40	1000	15.0	212	155	2320	4.25
Tube dia. 4 mm l = 28 cm							
1.67	0.60	500	50.0	398	109	5450	3.07
0.96	0.50	500	40.0	318	103	4120	2.32
Tube dia. 4 mm, l = 46 cm							
6.86	0.66	740	50.0	398	144	7200	9.50
5.60	0.66	740	40.0	318	138	5520	10.2
4.34	0.45	740	35.0	279	124	4350	10.0
1.17	0.26	592	20.0	159	114	2280	5.15
Tube dia. 3 mm, l = 46 cm							
1.47	0.37	667	50.0	177	101	5050	2.92
0.57	0.27	400	40.0	142	97	3880	1.47

trophoresis, plays an important role in continuous-radiation Ar^+ lasers. In the case of strong currents, the transfer of gas, usually proceeding from the cathode to the anode, reverses direction, and goes from the anode to the cathode. It was noted in[71] that in the continuous operation mode the laser generation appears only after a certain time after the start of the discharge. The experiments were performed with a tube of 8 mm diameter and l = 40 cm. The delay depends on the pressure and on the current, which determine the rates of transfer and forcing out of a gas. To equalize the pressure in the anode and cathode sections of the capillary and to ensure normal operation of the laser, the discharge tube is provided with a bypass channel. The diameter of the bypass channel is usually somewhat larger than the diameter of the capillary.

The theory of the gas-transport phenomenon in a discharge with large current density has been developed in[66,72]. In[66] are given also experimental data, which are compared with the theory.

An interesting experiment is described in[73], the authors of which obtained continuous laser operation in a continuous stream of argon. The argon could flow in the system either from the cathode to the anode or from the anode to the cathode. At discharge currents $i < 50$ A, the dependence of the power on the discharge current was the same (Fig. 15). At currents $i > 50$ A, the radiation power increases with the current if the gas flows from the cathode to the anode. When the gas flows from the anode to the cathode, the opposite picture is observed, and the radiation power decreases with increasing current.

c) Splattering of windows and mirrors. As indicated above, at the present time output powers up to 1 kW have been attained in an Ar^+ laser having a tube of 10 mm diameter and length ~3 m, in the blue-green region of the spectrum. Thus, at a mirror reflection coefficient of 90%, a power of ~1 kW falls on 1 cm^2 of the mirror. At powers of this order (at even at lower values, as follows from the data of[69]) the operation of the laser is particularly strongly influenced by the formation on the windows (or mirrors) of an absorbing layer consisting of splattered particles of the electrodes and the walls.

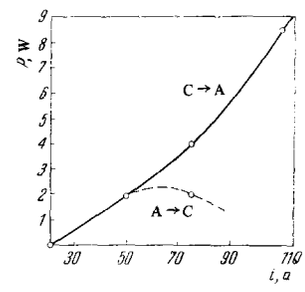

FIG. 15

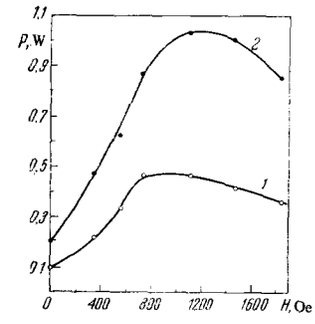

FIG. 16

FIG. 15. Dependence of the laser radiation power on the discharge current in the case of gas flow from the cathode to the anode (C → A) and from the anode to the cathode (A → C). Discharge tube of 6 mm diameter, L = 50 cm, p_0 = 0.5 Torr, H ~ 400 – 500 Oe.

FIG. 16. Dependence of the laser emission power on the external magnetic field at different transparencies of the laser windows.

As a result, the power of the laser decreases, the shape and dimensions of the nonlinear beam cross section change. After the absorbing layer is removed from the windows, the power of the laser and the beam shape and dimensions are restored. (Figure 16, taken from[69], shows the dependence of the output power on the external magnetic field. Curve 1 was obtained 50 hours after the start of the laser operation, and curve 2 immediately after the cleaning of the windows.)

The formation of an absorbing layer was investigated in detail in[74], where it was shown that absorption of the radiation in the absorbing layer results in thermal deformation of the optical elements located in the resonator, transforming them into a lens of sorts. This leads to a considerable divergence of the beam and to the limitation of the output power to a value much lower than obtained at the first instants of laser operation.

Among the measures proposed to prevent formation of an absorbing layer and the ensuing consequences are thorough outgassing of the discharge tubes and of all the parts, locating the cathode away from the discharge axis, locating the windows at larger distances

from the discharge, and the use of electric and magnetic fields as shutters in front of the optical part. Neither of these measures, however, is a reliable method of preventing formation of an absorbing layer. The absorbing layer on the surface of the windows (or on the internal mirrors) is the main obstacle limiting the increase of the power of the continuous Ar^+ laser. Owing to this layer, the actual service life of the windows (or mirrors) reduces to several minutes, thereby decreasing the actual usefulness of a 100-W continuous argon laser. In addition, the mirror layers of the resonator are damaged by the high-power laser radiation.

IV. HYPOTHESES CONCERNING THE MECHANISMS OF FORMATION OF INVERTED POPULATION IN AN ARGON ION LASER

In solving the problem of the mechanism of formation of inverted population in any laser system, it is necessary to answer two questions: 1) What processes ensure pumping to the upper laser level? 2) What processes are responsible for the decay of the population of the laser lower level?

For the Ar^+ laser, a practically unambiguous answer to the second question was obtained by Statz et al.[37], who established by calculation that the radiative lifetime of the lower laser levels of Ar II is much lower than that of the upper levels. From this, under the assumption (which, of course, must be verified) that the rates of pumping of the upper and lower laser levels do not differ very strongly, it follows that inverted population can be produced as a result of very intense transitions from the lower laser levels to the ground state of Ar II.

The situation is not so simple with the first question. As stated in Ch. II, the anser to this question could be proposed in the first investigations only in the form of hypothesis that called for experimental verification. Figure 17 illustrates the proposed hypothesis. Since all the laser lines of the ionic argon laser of continuous action belong to transitions between the configurations 4p and 4s, all the levels of each configuration are represented in the figure, for the sake of clarity, in the form of a single level. Using Fig. 17, let us discuss successively each of the hypothesis.

The hypothesis of Gordon and co-workers, that a stepwise excitation takes place (Fig. 17a) seems to be the most likely. Indeed, in order to excite the upper levels of the 4p configuration of Ar II from the levels of the ground configuration $3p^5$ of Ar II, it is necessary to have more modest electron temperatures than for excitation from the ground state of the atom of Ar I, $3p^6$, as is proposed in the hypothesis of Bennett et al. (Fig. 17d). The hypothesis of stepwise excitation is also confirmed by the experimentally-established approximately-quadratic dependence of the spontaneous emission of the laser lines of Ar II on the current density. It may seem that this hypothesis is contradicted by the fact that the electron cross section for the excitation of the upper laser levels in the configuration 4p of Ar II from the ground $3p^5$ configuration of Ar II should be much smaller in the Born approximation than the cross section for the excitation of the lower laser levels of the 4s configuration of Ar II,

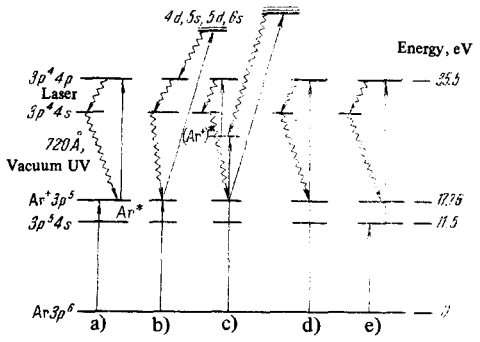

FIG. 17. Possible processes of population of laser levels of Ar II.

since the 4p levels have the same parity as the ground state. It must be borne in mind, however, that the Born approximation is not valid for the calculation of the cross section for the excitation of the ion levels. A definite role in the population of the levels of the 4p configuration may be played by cascade transitions from the levels ns ($n > 4$) and nd ($n > 3$) (Fig. 17b). Nor can one exclude the possibility of stepwise pumping by electron impact at several levels of the 4p configuration from the ground state of the argon ion via the metastable states located below the 4p configuration (Fig. 17c). In particular, levels of the 3d configuration of Ar II, with quantum number $J = {}^7/_2$ and ${}^9/_2$, which are not connected by optical transitions with the ground levels of Ar II, can take part in this process. The last two hypotheses were first mentioned in the paper of Bridges and Chester[20].

Bennett's hypothesis[21] that the upper laser configuration 4p of Ar II is populated directly from the ground state of the atom (Fig. 17d) is based on the fact that in collisions between fast electrons and atoms, of the type $e + Ar \rightarrow (Ar^+)^* + 2e$, the theory predicts a preferred population of the configuration $3p^44p$ of Ar II, compared with $3p^44s$. An analogous situation obtained also in the case of collision between electrons with metastable atoms (Fig. 17e)[4]. The hypothesis that the 4p configuration of Ar II is excited from the metastable state $3p^54s$ of Ar I has the advantage over the hypothesis of excitation from the ground state $3p^6$ of Ar I that in the former case less energy of the electrons is required than in the latter. This is quite important, for in the case of a continuous Ar^+ laser, unlike a pulsed one, one can hardly expect electron temperatures higher than 10 eV.

In the excitation of the levels of the upper laser configuration 4p of Ar II from the ground and the metastable states of Ar I, as well as of the levels of the lower laser configuration 4s from the ground state $3p^5$ Ar II, the absorption lines on the transitions $4s \rightarrow 4p$ will experience a Doppler shift relative to the initial lines, owing to the drift motion of the ions in the longitudinal electric field*. The presence of a Doppler shift between the upper and lower laser levels can lead to a decrease of the influence of the dragging of the radiation at the transition $4s \rightarrow 3p^5$, which is quite possible as a result of the high probabilities of

*It is assumed that the ions in the excited states are not additionally accelerated as a result of their brief stay in these states.

the radiative transition between the levels of these configurations. This means that the inversion between the 4p and 4s configurations can be retained up to arbitrarily large densities of Ar II, and consequently large specific powers of laser emission, as observed in experiment, can be attained.

The foregoing discussion illustrates that each of the proposed hypotheses concerning the mechanism of pumping and argon ion lasers has its shortcomings and advantages. Which of the hypotheses is reliable, or more accurately speaking, what role does each of the considered processes play in the formation of the inversion, cannot be ascertained without a quantitative or at least a semiquantitative analysis. Naturally, for this analysis it is necessary to have data on the parameters of the Ar^+-laser discharge plasma and on the rates of the radiative collision processes. Therefore we first discuss the results of measurements of the parameters of the plasma of an Ar^+ laser discharge.

V. PARAMETERS OF THE PLASMA OF AN IONIC ARGON LASER

1. Discharge Without Magnetic Field

The plasma of an argon discharge in capillaries, at low pressures, was first investigated in detail by S. E. Frish and his co-workers[75]. However, the current densities in the discharge, at which the investigations were performed, did not exceed 50 A/cm^2, i.e., they were much lower than the densities characteristic of Ar^+ lasers.

Information concerning the parameters of the Ar^+ laser plasma, when the laser is fed with direct current, were obtained in[76-87], mainly by the spectral-diagnostics method. Investigations other than spectral were performed only in the Bell Laboratories, where probe measurements were made, but at current densities much lower and gas pressures much higher than those at which generation is observed. The details of these investigations have not yet been published, but the results of the measurements are cited by Chester[66] in the form of empirical formulas for the temperature of the gas and the electron density. Great interest attaches to the work of V. A. Stepanov and co-workers[86], who investigated the distribution of the gas density in the Ar^+ laser capillary by an interferometric method with an He-Ne laser used as the light source.

Spectral investigations were carried out at the Physics Institute of the USSR Academy of Sciences[76,80] in quartz tubes of two types, under conditions typical of Ar^+ lasers. The length and diameter of one tube were 25 and 1.6 mm, and that of the other were 40 cm and 2.8 mm. The capillary and the anode were cooled with water. The current density ranged from 100 to 500 A/cm^2, and the pressure ranged from 0.1 to 0.7 Torr.

a) The atom temperatures determined from the Doppler width of the Ar I lines emitted along the discharge range from 1500 to 3500°K (Fig. 18). The Ar II lines also have Doppler contours, but the longitudinal ion temperatures $T_{\parallel}^*$ are higher than the atomic ones by an approximate factor of 1.5. The transverse temperature $T_{\perp}^*$ is still higher than the longitudinal ion temperature. Thus, the velocity distributions of the ions and atoms are different, and in addition, the ion velocity distribution is anisotropic in space. With increasing current density, both the atom and the ion temperature increase. The dependence of the atom temperature on the pressure is relatively weak, while the ion transverse temperature increases quite strongly when the pressure changes from 0.2 to 0.37 Torr. At the same current densities, the temperature of the atoms in a capillary of 2.8 mm diameter is higher than that in one of 1.6 mm diameter.

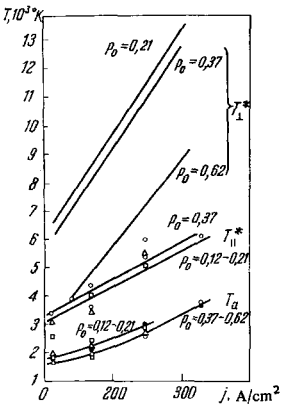

FIG. 18. Dependence of the temperature of the atoms T_a, of the longitudinal temperature $T_{\parallel}^*$, and of the transverse temperature $T_{\perp}^*$ of the ions on the current density for a tube of 2.3 mm diameter. p_0 – filling pressure. The temperature of the atoms was measured from the Ar I 4259 and 4272 Å lines, the temperature of the ions from the Ar II Å 4933 and 4228 Å lines. ($T_{\parallel}^*$ – from radiation along the discharge, $T_{\perp}^*$ – from radiation across the discharge; the experimental points for the dependence of $T_{\perp}^*$ on j are not indicated, since they are derivatives of the dependences of $\delta\lambda_{\perp}^*$ on j, constructed from the experimental data).

The obtained values of the atom temperature in the plasma of the Ar^+ laser agree with the data of[81,82], and, somewhat surprisingly, the experimental values of T_a for the capillary with 2.8 mm diameter agree with those calculated in accordance with Chester's empirical formula[66]

$$T_a/300 = 1 + 2j\,(\text{A/mm}^2)\,D^{1/2}\,(\text{mm})^{1/2}, \qquad (3)$$

In spite of the fact that T_a was obtained on the basis of experiments performed in a different range of currents and pressures to the experiments performed at Physics Institute of the USSR Academy of Sciences. The agreement is somewhat worse for a capillary with D = 1.6 mm (the calculated values are higher than the experimental ones by 20–30%).

b) The concentration of the argon atoms in the discharge in the capillary is much lower than the concentration of the initial gas filling the tube, since the strong heating of the gas in the capillary ($T_a \sim 1600$–3600°K) causes it to be forced out into parts of the discharge that are colder and larger in volume (the anode and cathode bulbs). At a known atom temperature, the concentration of the argon atoms can be estimated on the basis of the gas law

$$N = N_0 \cdot 300/T_a \qquad (4)$$

(where N_0 is the concentration of the atoms at room temperature), and the mean free path of the atom can be determined with the aid of the formula[66]

$$\lambda_a = 0.0476\,(T_a/300)/p. \qquad (5)$$

If it is assumed that the concentration of the argon atoms during the time of filling is 1.3×10^{16} cm^{-3} (p_0 = 0.37 Torr), then, as follows from Fig. 18, for a capillary with r = 1.4 mm it will be equal to 2.7×10^{15} cm^{-3} at j = 160 A/cm^2, and 1.1×10^{15} cm^{-3} at j = 330 A/cm^2, while the mean free paths of the atoms will be 0.7 and 1.5 mm, respectively. These estimates show that at capillary radii, pressures, and current densities characteristic of the argon laser, the mean free path turns out to be comparable with the radius of the capillary. If this is so, then the applicability of the gas law to the estimate of the concentration becomes doubtful. There is all the more reason for the doubt, since no account is taken of the pressure of the electron gas, which may be comparable with the pressure of the neutron gas as a result of the high temperature T_a (see below).

In addition, experiments have shown[82,88] that at large currents a radial inhomogeneity of the atom concentration sets in. This agrees with the theory of Caruso and Cavaliere[89], according to which the degree of inhomogeneity of the plasma depends on the quantity $N_e\langle v_e\sigma_e\rangle_i r/v$ (N_e–electron density, v $\langle v_e\sigma_e\rangle_i$–averaged rate of ionization by the electrons, r–radius of the capillary, v–thermal velocity of the atoms). In the case of the discharge used for Ar^+ lasers, this quantity is of the order of unity. In the presence of an appreciable radial inhomogeneity, we do know the ratio of the concentration obtained with the aid of the gas law to the concentration existing in the discharge. However, measurements of Stepanov and co-workers[82] have shown that approximately at the midpoint of the capillary radius the concentration of the neutral atoms coincides with that calculated in accordance with a gas law. Therefore, for estimates of the average concentrations of the atoms in the plasma of an ionic argon laser we can use the gas law.

The mean free path of the argon ion between charge exchanges[66], i.e.,

$$\lambda_i \approx 0.05\,(T_a/300)/p, \qquad (6)$$

is approximately equal to the mean free path of the argon atom. This leads to the important conclusion that not only $\lambda_a \approx r$, but also $\lambda_i \approx r$, and that in the first approximation the ions therefore fall freely on the wall.

c) The temperature of the electrons in the laser plasma can be determined on the basis of the Langmuir-Tonks-Klyarfel'd (LTK) theory. To be sure, the values of K_e determined in this manner will be only tentative, since the LTK theory is valid if $\lambda_i > r$, but not when $\lambda_i \sim r_i$, as is the case in the discharge. Figure 19 shows the dependence of the electron temperature T_e on rp_0 (p_0–pressure in the capillary at 0°C), calculated in accordance with the Klyarfel'd formula[90] at $C_i = 0.70$[91].

It follows from the diagram that for a capillary of 2.8 mm diameter and at a filling pressure p_0 = 0.37 Torr, the value of T_e increases from 43,000 to 52,000°K when the current density increases from 160 to 320 A/cm^2.

The increase of T_e with increasing current density is due to the decrease of the gas density as a result of the decrease of T_a, which leads to a further forcing out of the gas. As already indicated above, the obtained value of T_e should be regarded only as an estimate. It is tentative also because it was assumed, in the calculation by the Klyarfel'd formula, that the ionization occurs from the ground state, whereas ionization from the metastable state can also be appreciable. Furthermore, in the LTK theory it is assumed that the gas density in the gas-discharge tube is constant, whereas there is an appreciable density gradient in the discharge of interest to us.

An estimate of the electron temperature of the Ar^+ laser plasma can also be obtained on the basis of experimental data on the ion transverse temperature from the Kagan-Perel' theory[92]. The large broadening of the ion lines compared with the atom lines in the discharge of interest to us is connected with the presence of radial and longitudinal electric fields. The larger the radial field, the broader the ion line observed in a direction perpendicular to the discharge axis. On the other hand, according to Langmuir and Tonks, the radial potential difference V_r is connected with the electron temperature T_e by the simple relation

$$eV_r = 1.1kT_e. \qquad (7)$$

This formula expresses the simple fact that to ensure equality of the electron and ion currents to the wall the radial field must delay the bulk of the electrons from the Maxwellian distribution. It is seen from (5) that the larger T_e the larger V_r, and consequently the larger the width of the ion line observed in the transverse direction. Kagan and Perel'[92] solved the kinetic equation under the condition $\lambda_i > r$, and obtained the ion-velocity distribution function in a cylindrical discharge tube. The solution was obtained with allowance for the longitudinal and transverse electric fields, under the assumption that the ions are produced in the volume and vanish on the walls. It was also assumed that the excited states of the ions originate from the ground state. Using the ion velocity distribution function, Kagan and Perel' calculated the effective transverse ion temperature $T_\perp^*$, which can be determined from the width of the ion lines registered by observation along the capillary diameter, and found that it is connected with T_e and T_a by the relation

$$T_\perp^* = 0.56T_a + 0.13T_e. \qquad (8)$$

Table III lists the results of an estimate of T_e in accordance with formula (8) as a function of the current density for three pressures in a capillary of 2.8 mm diameter. The initial data are the half-widths of the spectral lines of Ar II and the effective transverse temperatures calculated from them (see Fig. 18)*. Estimates show that the electron temperature increases with the current density and decreases with increasing pressure. Thus, at a pressure p_0 = 0.37 Torr, when the current density increases from 160 to 330 A/cm^2 (in a capillary of 2.8 mm diameter), T_e increases from 52,000 to 90,000°K, and at j = 160 A cm^2 it drops from 56,000 to 32,000°K when the pressure

*We note that the Lorentz part was not separated from the experimental Ar line widths, so that the value of T_e listed in Table III are somewhat overestimated.

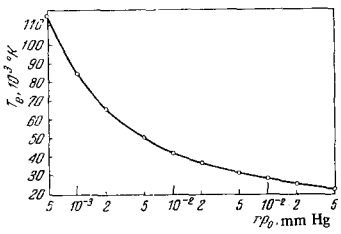

FIG. 19. Dependence of T_e on rp_0 in accordance with the theory of Langmuir-Tonks-Klyarfel'd. r – tube radius, p_0 – pressure at 0°C.

Table III. Electron temperature T_e in the plasma of a discharge in argon in a capillary of 2.8 mm diameter

j, A/cm²	T_e, 10^4 °K		
	$p_0 = 0.21$ Torr	$p_0 = 0.37$ Torr	$p_0 = 0.62$ Torr
160	5.6	5.2	3.2
200	6.5	6.1	4.0
240	7.3	6.9	4.7
300	8.6	8.3	5.9
330	9.2	9.0	6.5

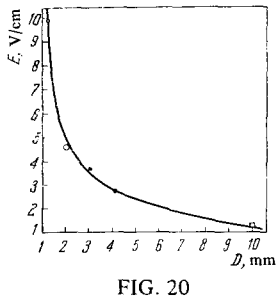

FIG. 20

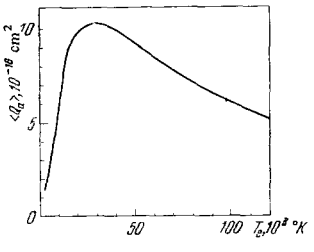

FIG. 21

FIG. 20. Longitudinal electric field E as a function of the capillary D. ● – from [27] (i = 5 – 16 A, p_0 = 0.12 – 0.50 Torr), ○ – from [45] (i = 9 A, p_0 = 0.2 Torr), □ – from [40] (i = 100 A, p_0 = 0.05 Torr).

FIG. 21. Dependence of the cross section of the electric conductivity $\langle Q_a \rangle$ on T_e.

increases from 0.21 to 0.62 Torr. The growth of the temperature with increasing current density is perfectly understandable, if it is recognized that the gas density decreases with increasing j, so that the mean free path λ_e increases, and with it also T_e, in accordance with the relation[93]

$$T_e = E\lambda_e/\sqrt{2\varkappa}, \tag{9}$$

($\varkappa$ is the fraction of the energy lost on the average by the electron in one collision). Thus, the growth of T_e takes place in spite of the fact that the field intensity remains constant.

d) The electron concentration N_e at a known electron temperature can be estimated with the aid of the electric-conductivity formula[94]

$$\sigma = \frac{j}{E} = \frac{407 N_e K_\sigma(0)}{T_e^{1/2}\left[N_i\langle Q_i\rangle + N_a\langle Q_a\rangle\right]}. \tag{10}$$

j is a known quantity, E is determined from the plot in Fig. 20, which is based on the data of[34,47,52], N_i and N_a are the ion and atom concentrations in the discharge, and $\langle Q_i \rangle$ and $\langle Q_a \rangle$ are the corresponding electric conductivity cross sections; $K_\sigma(0) \sim 1$. The electric-conductivity cross sections $\langle Q_a \rangle$ as functions of T_e were calculated by P. L. Rubin and are given in Fig. 21. At $T_e = 5 \times 10^4$°K we have $\langle Q_a \rangle = 8 \times 10^{-6}$, and at $T_e = 9 \times 10^4$°K we have $\langle Q_a \rangle = 6 \times 10^{-16}$ cm². The $\langle Q_i \rangle$ were calculated from the formula[95]

$$\langle Q_i \rangle = \frac{20{,}2\cdot 10^{-6}}{T_e^2}\lg\left[\frac{279 T_e}{N_e^{1/3}}\left(\frac{T_a}{T_a + T_e}\right)^{1/3}\right]. \tag{11}$$

The results of the calculation of N_e are given in Table IV. It must be recognized that the estimate of N_e with the aid of formula (10) has an accuracy not better than by a factor of 2. This is connected primarily with the insufficient accuracy with which the argon atom concentration is determined. However, an estimate of N_e on the basis of the half width of the H_β line confirms the assumption that the data listed in Table IV are reasonable.

As seen from Table IV, N_e varies little with variation of j. To the contrary, it increases from 3×10^{13} to 14×10^{13} cm^{-3} with increasing pressure from 0.21 to 0.62 Torr.

In addition to the values of N_e obtained from the data on the electric conductivity, Table IV lists the values of N_e obtained from Chester's empirical formula[66]

$$N_e(\text{cm}^{-3}) = 10^{13} j\ (\text{A/cm}^2)\, r\ (\text{cm})\, p_0\ (\text{Torr})\,(300/T_a)^{1/2}. \tag{12}$$

In spite of the fact that Chester's formula was obtained on the basis of experiments with a discharge at higher pressures and lower current densities than those that are typical in Ar^+ lasers, there is agreement, with accuracy not larger than by a factor of 2, between the data obtained from the electric conductivity and with the aid of Chester's formula, which has been derived on the basis of experiments performed at the Bell Laboratories.*

Summarizing, we can state that the data obtained by various authors concerning the temperatures of the atoms and the concentrations of the electrons are in satisfactory agreement. With respect to T_e, on the other hand, there is an appreciable discrepancy between the data of FIAN and the data of the Bell Laboratories. As seen from the Physics Institute (FIAN) data listed in Table III, the temperature estimated from the half-widths of the lines radiated across the discharge, under conditions typical of the operation of Ar^+ lasers, increases with increasing current density from 50,000 to 90,000°K at p_0 = 0.21–0.37 Torr, and from 30,000 to 60,000°K at p_0 = 0.62 Torr. We emphasize that the growth of T_e with increasing current density is a reliably established fact, but the accuracy with which the absolute values of T_e have been determined is not too high (~20%), in view of the fact that the Kagan-Perel' theory is based on a model.

On the other hand, according to the measurements performed at the Bell Laboratories[87,66], the value of

*We note that the agreement is only with respect to the value of N_e, but not with respect to the dependence of N_e on j. According to formula (12), $N_e \sim j^{1/2}$ (since $300/T_a \sim j^{-1/2}$). In the investigations performed at the Physics Institute of the USSR Academy of Sciences (FIAN), in the narrow range of j in which the investigations were carried out, no dependence of N_e on j was observed within the limits of the experimental errors.

Table IV. Electron concentration N_e in the plasma of a discharge in argon in a capillary of 2.8 mm diameter

j, A/cm²	T_a, °K	N_e, 10^{13} cm^{-3}						
		$p_0 = 0.21$ Torr		$p_0 = 0.37$ Torr			$p_0 = 0.62$ Torr	
		From σ	From formula (12)	From σ	From formula (12)	From the half-width of Hβ	From σ	From formula (12)
160	1900	2.9	1.9	5.4	3.3	—	14.4	5.5
200	2300	3.0	2.1	5.4	3.7	3.7	13.3	6.3
240	2700	3.0	2.3	5.5	4.1	—	14.3	6.9
300	3300	3.0	2.7	5.5	4.7	—	13.4	7.9
330	3700	2.9	2.8	5.2	4.9	—	13.0	8 1

T_e in the discharge used for Ar^+ lasers is of the order of $(20-25)\times 10^3$°K and does not depend on j. It is impossible to agree with this result, since at these temperatures one cannot ensure the generation powers observed experimentally (see below) even at large ion concentrations N_i (exceeding 2×10^{14} cm^{-3}).

e) The ionization rate z, i.e., the number of ionizations per second in 1 cm^3 per electron, is an important characteristic of the plasma and is a quantity inverse to the lifetime of the ion in the discharge. According to the Langmuir-Tonks theory, it equals

$$z = (S/\rho)\,(M/2kT_e)^{-1/2}. \qquad (13)$$

On the plasma boundary $\rho = r$ and $S = 0.77$. This relation expresses the simple physical fact that accurate to a coefficient of the order of unity, the reciprocal time of flight of the ion from the axis to the wall is equal to the velocity of its motion as determined by the radial field ($ev_\perp = kT_e$), divided by the radius of the tube.

According to the Kagan-Perel' theory, when $\lambda_i \gtrsim r$ it is possible to determine z from the experimentally measured ion drift velocity v_z with the aid of the relation

$$\bar{v}_z = 0.69eE/M_i z. \qquad (14)$$

Thus, the drift velocity is proportional to the longitudinal field E and to the lifetime of the ion in the discharge; the larger the radial field, the smaller this lifetime.

The drift velocity of the ions and atoms along the tube was determined by measuring the Doppler shift of the spectral line of Ar^+. The optical system of the setup is shown in Fig. 22. The results obtained for the ion and atom velocities, for a tube of 2.8 mm diameter, are shown in Figs. 23 and 24. As seen from Figs. 23 and 24, the drift velocities of the atoms and of the ions are of the same order of magnitude. However, with increasing current, the ion drift velocity decreases and the atom drift velocity increases. These results are perfectly understandable. If $\lambda_i \sim r$, the observed decrease in the ion drift velocity with increasing current density is connected with the increase of the acceleration of the ions towards the wall as a result of the increase of the radial field. The existence of an atom drift towards the anode agrees with the experimentally observed transfer of gas from the cathode to the anode as a result of the dragging of the atoms by the electron stream. As follows from Fig. 23, the momentum transferred to the electrons (per atom) increases with increasing current density j, this being connected with the decrease of the gas density with increasing j.

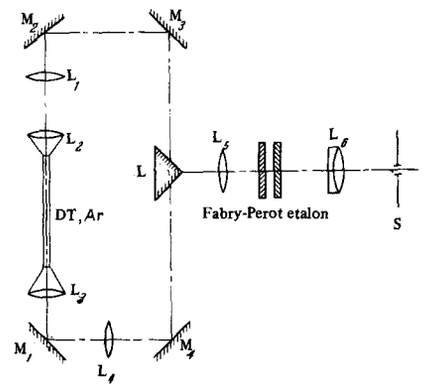

FIG. 22. Optical system of the setup for the measurement of the Ar Ar I and Ar II line shifts. M_1, M_2, M_3, M_4 – mirrors, P – prism, DT – discharge tube, L_1, L_2, L_3, L_4, L_5, L_6 – lenses, s – slit of UF-90 camera.

The possible drift of the atoms does not take into account in the Kagan-Perel' theory, so that $\bar{v}_z$ in formula (14) is simply equal to the ion drift velocity. In our case, however, the ions come from atoms moving in a direction opposite to the field; therefore $\bar{v}_z$ in (14) is equal to $\bar{v}_z = \bar{v}_i + \bar{v}_a$, where $\bar{v}_i$ and $\bar{v}_a$ are the ion and atom velocities determined from the shift of the spectral lines of the ions and the atoms. The ionization rate was determined from the velocity $\bar{v}_z$ in accordance with formula (14). The obtained results are listed in Table V (for a tube of 2.8 mm diameter). The same table gives the results of the calculation of z in accordance with the Langmuir-Tonks theory, using the experimental values of T_e from Table III. As seen from Table V, the agreement between the two values of z is satisfactory, thus clearly indicating that the estimates of T_e given in Table III are reasonable. Measurements were also made at FIAN of the shift of the Ar II lines in a capillary of 1.6 mm diameter, up to a current density 500 A/cm^2. These measurements have shown that in this capillary z is larger than in the 2.8 mm capillary, and reaches $(1-2)\times 10^7$. We emphasize that the values of z given in Table V, just like the values of T_z in Table III, are estimates, in view of the complexity of the investigated discharge as compared with the discharge model on which the theories of Langmuir-Tonks and Kagan-Perel' are based.

Notice must be taken of two other circumstances. First, according to the theory of Kagan and Perel', z can be determined not only from the shift of the ion lines, but also with the aid of the formula

$$T_{\parallel}^* = T_a + (0.82e^2E^2/kMz^2), \qquad (15)$$

where $T_{\parallel}^{*}$ is the temperature determined from the Doppler width of the ion line, observed along the discharge. In spite of the fact that this formula does not take into account the generation of the ion by an atom having a velocity directed opposite to the longitudinal field, estimates based on this formula give values that are underestimated by not more than 2—3 times compared with the estimates of z by formula (14).

Second, in the discharge of interest to us, z can be calculated from the known temperature of the electrons and the ionization cross section. Calculations carried out by P. L. Rubin, with allowance for the fact that ionization is appreciable not only from the ground state of the argon but also from the metastable state, have shown that the values of z obtained in this manner are larger by 3—10 times than those given in Table V. A discrepancy of this type may be connected with the insufficient reliability of the employed cross section for the ionization from the metastable state. We therefore regard the estimates of z given in Table V as more reliable.

2. Discharge in a Longitudinal Magnetic Field

Inasmuch as superposition of an external longitudinal magnetic field leads to an appreciable increase of the output power of the Ar^{+} laser, there is a justified interest in elucidating the physical processes that lead to this effect, primarily in the dependence of the parameters of the laser discharge plasma on the magnetic field. In experiments carried out at FIAN, they investigated the influence of the magnetic field of the temperature of the atoms (T_a) and on the drift velocities of the atoms and ions. The temperature was determined from the Doppler broadening of the spectral lines, measured with the aid of a Fabry-Perot interferometer crossed with a diffraction spectrograph. The optical system of the experimental setup is shown in Fig. 25. When experiments are performed with a magnetic film, it is necessary to bear in mind that the magnetic field leads to a splitting of the spectral lines. Lines were therefore chosen, for which the g-factors of the upper and lower states are equal; then a doublet is observed along the field, and one of the components of the doublets can be separated with the aid of an achromatic quarter-wave plate (Fresnel prism) and a polaroid filter. The ion line chosen was λ 5145 Å ($g_1 = g_2 = 1.334$). The preferred atom line was λ 4158 Å, whose g-factors are close to each other ($g_1 = 1.420$, $g_2 = 1.506$), and the fine structure of the Zeeman splitting could be neglected within the limits of the experimental error. The measurements were performed in a magnetic field at an intensity close to optimal for generation, and equal to 700 Oe. The measurements have shown that the temperatures of the atoms, following application of the field, remains constant and the longitudinal "temperature" of the ions T_i decreases by not more than 10—15%, while the ion and atom drift velocities decrease by approximately 10%, i.e., a magnetic field of 700 Oe does not change these plasma parameters appreciably. On the other hand, the intensity of the spontaneous-emission lines of the argon atoms decreased by approximately one-half, which clearly points to a change of T_e and N_e

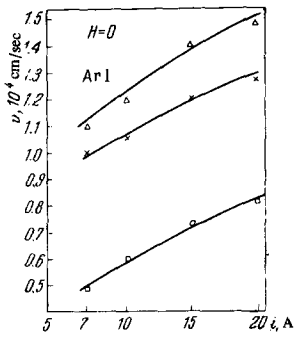

FIG. 23

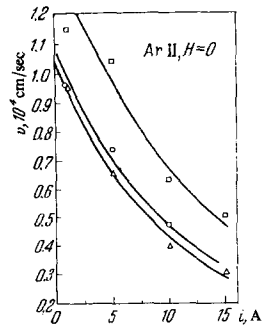

FIG. 24

FIG. 23. Drift velocity of the atoms against the discharge current for a tube of 2.8 mm diameter. Δ – p_0 = 0.12 Torr, × – p_0 = 0.36 Torr, □ – p_0 = 0.62 Torr.

FIG. 24. Drift velocity of the ions against the discharge current for a tube of 2.8 mm diameter. □ – p_0 = 0.62 Torr, ○ – p_0 = 0.36 Torr, Δ – p_0 = 0.12 Torr.

Table V. Ionization rate z as a function of the current density for a tube of 2.8 mm diameter

j, A/cm²	z, 10⁶ ionizations/electron-sec-cm³					
	p_0 = 0.21 Torr		p_0 = 0.37 Torr		p_0 = 0.62 Torr	
	From the line shift	From T_e	From the line shift	From T_e	From the line shift	From T_e
100	3.0	—	3.2	—	3.6	
160	3.3	2.6	3.5	2.5	3.9	2.0
200	3.4	2.8	3.6	2.8	4.2	2.2
240	3.4	3.0	3.7	2.9	4.3	2.4
300	3.4	3.3	3.8	3.2	4.2	2.7
330	3.5	3.4	3.8	3.3	4.1	2.8

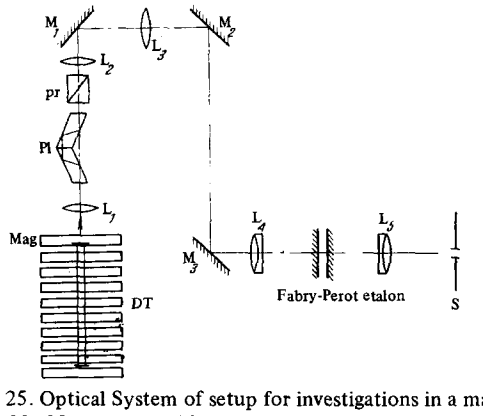

FIG. 25. Optical System of setup for investigations in a magnetic field. M_1, M_2, M_3 – mirrors, Mag – magnet, DT – discharge tube, Pl – quarter-wave plate, Pr – polaroid filter, L_1, L_2 – objectives, S – slit of UF-90 camera.

with increasing H. The following can be said concerning these discharge parameters, which determine the rate of pumping at the upper and lower laser levels:

When a magnetic field is applied to a discharge satisfying the condition $\lambda_i \gtrsim r$, according to J. Forrest and R. Franklin[96], the rate of diffusion of the electrons towards the wall decreases, leading to a decrease and to a modification of the radial potential. As a result, the rate of ionization and the electron temperature de-

Table VI

H, Oe	z, 10^6 sec^{-1}	T_e, °K	H, Oe	z, 10^6 sec^{-1}	T_e, 10^3 °K
0	2.5	52	330	0.81	41
185	1.8	48	560	0.31	35
300	0.95	42	680	0.25	33

crease. Table VI illustrates the dependence of T_e and of z on H. The initial values of T_e and z were chosen to be the experimental data at H = 0 for a capillary with 2.8 mm diameter at $p_0 = 0.37$ and $j = 160$ A/cm^2, for which $T_a = 1800$°C and $T_e = 52{,}000$°K. The foregoing data were obtained by Yu. A. Pekar and P. N. Zakharov in accordance with the theory of Forrest and Franklin. It follows from Table VI that when the magnetic field increases from zero to 680 Oe, the electron temperature decreases from 52,000 to 33,000°K.

The influence of the magnetic field on the operation of the continuous argon ion laser was investigated experimentally in[88]. The diameter of the capillary in this investigation was 1–38 mm, the discharge current was 5–20 A. When the magnetic field intensity was increased from 0 to 700 Oe, the value of T_e decreased from 4×10^4 to 2.6×10^4°K. The concentration of the electrons increase with increasing field. Estimates were made of the populations of the laser levels. They have shown that the inversion density depends on the field nonmonotonically: there is a maximum in the region 2–4 kOe.

As seen from the foregoing, the strong-current arc discharge of the Ar^+ laser has a number of peculiarities and is difficult to understand. The presence of large radial fields and the associated deviation from isotropy and of the Maxwellian velocity distributions of the ions and the electrons, the high gas temperature, the forcing out of the gas from the capillary and its transfer, the appreciable radial inhomogeneity of the gas density, and also the fact that the particle mean free paths are of the same order as the capillary radius, all make it difficult to construct for such a discharge a theory that is anywhere nearly complete. Therefore, for quantitative description of the characteristics of the discharge and of the processes leading to the formation of inversion in Ar^+ lasers, it becomes necessary to use highly simplified models of the discharge, for which calculations can be performed, and to check the applicability of the chosen models by comparing the theoretical results with experiment. Among the usually employed simplifications are neglect of the radial inhomogeneity of the discharge, the assumption that the electron energy distribution is Maxwellian, the use of the results of the Langmuir-Tonks theory, in spite of the fact that the condition $\lambda_i \gg r$ is not satisfied, and a number of others.

The material presented in this chapter shows that considerable progress has been made in the study of the gas discharge of an Ar^+ laser without a magnetic field. At the same time, the discharge with a magnetic field, its main parameters, the concentration T_e, and the very mechanism of the action of the magnetic field on the discharge, leading to an increase of the inversion and of the output power of the Ar^+ laser, have not been investigated to a sufficient degree at all. For a further experimental investigation of the parameters of Ar^+ laser discharge, particularly, in the presence of a magnetic field, it is desirable to employ new plasma-diagnostics methods, particularly microwave methods.

VI. PROBABILITIES OF RADIATIVE TRANSITIONS AND RATES OF ELECTRON EXCITATION OF THE ARGON ION

The fundamental configuration $3p^4$ of the doubly-charged argon ion corresponds to the terms ^3P, ^1S, and ^1D. According to Hund's rule, the ground term of Ar^{III} is ^3P, above which is located the term ^1D, followed by the term ^1S. Accordingly, the singly-charged Ar II ion will have three systems of terms with the terms of the ionic residue ^3P, ^1S, and ^1D. Since the principal generation transitions of a continuous laser are transitions between the variables with the ionic residue ^3P, we are interested only in this group of levels. The possibility of considering processes occurring between levels having one ionic residue, neglecting the transitions between the system of levels with different ionic residues, is due to the fact that the probabilities of the transitions, both radiative and electron-collision, between systems of terms will be much less than the probabilities of transitions within the confines of each system.

The ground configuration of Ar II is $3p^5$ with the levels $^2P_{1/2,3/2}$. The upper laser configuration is $3p^44p$, and the lower one is $3p^44s$. The excited configurations $3p^2nl$ of Ar^{II} correspond to doublet and quartet terms. Belonging to the configuration $3p^44s$ are the levels $^2P_{1/2,3/2}$ and $^4P_{1/2,3/2,5/2}$, and to the configuration $3p^44p$ are the levels $^2S_{1/2}$, $^2P_{1/2,3/2}$, $^2D_{3/2,5/2}$, and $^4S_{3/2}$, $^4P_{1/2\ 3/2\ 5/2}$, $^4D_{1/2,3/2,5/2,7/2}$. Figure 26 shows the energy scheme of the configurations of Ar II. The numbers at the arrows between the configurations give the average values of the radiative probabilities of the transitions, calculated by Statz et al.[37], with the

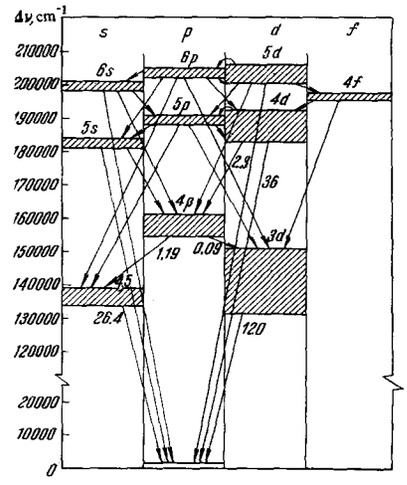

FIG. 26. Diagram of electronic configuration of the argon ion. The numbers at the arrows designate the radiative probabilities of the transitions in units of 10^8 sec^{-1}.

values of the probabilities of the transition to the main configuration, corrected by P. L. Rubin[98]*. The spin forbiddenness for radiative transitions from the quartet term $3p^4 4s\,^4P$ to the ground doublet term is not rigorous, since for this configuration the LS coupling is valid only approximately[37]. However, the probability of transitions from $4s^4P$ to the ground state is smaller by two orders of magnitude than the transition probability shown in Fig. 26 for $4s^2P$. Nor is the spin forbiddenness fulfilled for transitions between excited configurations, but the probabilities of the transitions between the quartet and doublet excited configurations is smaller by one order of magnitude than within the confines of each of the group of levels of one multipolarity[37]. Violation of the selection rule with respect to spin indicates, as noted above, that the probabilities of the transitions between the excited levels of Ar II cannot be calculated in the LS coupling approximation. It is necessary to use an intermediate type of coupling, as was done by Statz et al.[37], and later by H. Marantz[99] in the calculation of the probabilities of the transitions both between the doublet and quartet levels, and for the intercombination transitions between them. A comparison of these calculations of the experimental data has shown a perfectly satisfactory agreement between theory and experiment[37,100]. Since we shall need in the subsequent discussion only the average probabilities of the transitions between the configurations (and not between the levels), we confine ourselves to the average transition probabilities given in Fig. 26 for configurations only†. As seen from Fig. 26, the probabilities of the transitions from the configurations 3d, 4s, 4d, to the ground configuration are equal respectively to 120, 26, and 36 (in units of 10^8 sec^{-1}). These values pertain, of course, to transitions from the doublet levels. The probabilities of the 4p → 4s and 4d → 4p transitions are equal to 1 and 2.4 (in units of 10^8 sec^{-1}), and are the same both between quartet and between doublet levels. We emphasize that the corrected values for the transition probabilities 4s → 3p are in good agreement with the results of Bennett[85], who measured the Lorentz width of the λ 4880 Å line and found that it is five times larger than the value expected for the natural width in the case of the 4s → 3p transition probability given in[37]. The cross sections σ_e for the excitation of Ar II by electron impact were calculated numerically[106] in the Born-Coulomb approximation, in which the external electron is described by Coulomb functions of the continuous spectrum. In this approximation, the effective cross section for the excitation of the configuration

*There are a number of misprints in the article of Statz et al., who calculated for the first time the probabilities of the Ar II transitions. In the caption of Fig. 1 of this article it is indicated that the probabilities of the transitions are in units of 10^7 sec^{-1}. Actually they are expressed in units of 10^8 sec^{-1}. A value of 2.4×10^7 sec^{-1} is then given for the probability of the 3d → 3p transition, whereas the correct value is 24×10^8 sec^{-1}. Finally, for all transitions to the ground state, the transition probabilities are underestimated by a factor of 5, since the authors have left out the factor 5 connected with the number of equivalent electrons. Our Fig. 26 incorporates all the corrections, which have been reconciled with Statz's data.

†The transition probabilities, the level life-times, and the excitation cross sections of ArII are dealt also in [101-105].

Table VII. Values of $\langle v_e\sigma_e \rangle$ (in units of 10^{-10} cm^3/sec) for the configurations of Ar^+

Transition \ T_e, 10^4 °K	2	3	5	8	10
$3p - 4p$	$4.7 \cdot 10^{-3}$	0.18	3.0	14	23
$3p - 3d$	$0.99 \cdot 10^{-1}$	3.0	44	190	300
$3p - 4d$	$0.97 \cdot 10^{-3}$	0.078	2.4	16	28
$3p - 5d$	—	0.0047	0.22	1.8	3.4
$3p - 4s$	—	0.23	2.7	11	17
$3p - 5s$	—	0.003	0.10	0.62	1.1
$3d - 4p$	$9.3 \cdot 10^2$	1900	2000	2000	1900
$4s - 4p$	$3 \cdot 10^3$	4800	6600	7700	8000
$4s - 3d$	$8.2 \cdot 10^2$	—	—	—	—

does not depend on the coupling scheme of the atomic electrons. Semiempirical radial functions[107] were used in the calculations. The calculation of the cross sections between the individual levels of the configurations was not carried out, since it requires in the case of Ar II the use of an intermediate coupling scheme, which is a very laborious task. In Table VII are given values of $\langle v_e\sigma_e \rangle$ of the rate of excitation ar Ar II from the ground to the excited states, calculated for one electron and one ion. $\langle v_e\sigma_e \rangle$ denotes the averaging of the cross sections σ_e over the Maxwellian distribution of the velocities v_e. The values of $\langle v_e\sigma_e \rangle$ listed in the table pertain to all three (^3P, ^1D, and ^1S) ionic residues. The group of terms connected with the ionic residue ^3P corresponds to the value equal to $3/5$ of $\langle v_e\sigma_e \rangle$ listed in Table VII. As seen from the table, at temperatures from 33,000° to 100,000°K the rates of population from the ground state of the configurations $3p^4 4s$, $3p^4 4p$, and $3p^4 4d$ are practically the same and increase in the indicated limits from 10^{-11} to 10^{-9} cm^3/sec. A very sharp decrease of $\langle v_e\sigma_e \rangle$ (by almost two orders of magnitude) is observed for these transitions when the temperature is decreased from 30,000 to 20,000°K. The rate of population from the ground state of the configurations $3p^4 3d$ is higher by one order of magnitude, and that of the 5s and 5d configurations is smaller by one order of magnitude or even two orders of magnitude than $\langle v_e\sigma_e \rangle$ for the configurations 4s, 4p, and 4d. The rates of excitation of the laser configuration 4p from the configurations 3d and 4s is of the order of 10^{-7} and is practically independent of the temperature, as is also the case for $\langle v_e\sigma_e \rangle$ for the 4s → 3d transition.

VII. MECHANISM OF FORMATION OF INVERTED POPULATION

Let us consider the role of different processes in the creation of the inverted population in Ar^+ lasers. In Table VIII are given the results of the calculation of the rates of pumping and populations of the configurations of Ar II at three pressures of Ar and at two current densities, for which experimental values of N_e and T_e are available for a discharge in a capillary of 2.8 mm diameter, and given in the third column of the table. In the next two columns are given the pumping rates of the configurations 4s and 4p (or only of doublet terms with atomic residue ^3P) from the ground configuration $3p^5$ of Ar II. The calculation was carried out for each regime by multiplying N_e^2 by the values of $\langle v_e\sigma_e \rangle$ obtained by interpolation from the

Table VIII

p_0, Torr	j, A/cm²	T_e, 10^4 °K; N_e, 10^{13} cm⁻³	Pumping rate, 10^{17} cm⁻³ sec⁻¹				Total pumping rate, 10^{17} cm⁻³ sec⁻¹		Population of configuration, 10^9 cm⁻³		Population of doublet system per USW, 10^8 cm⁻³		Inversion per USW, 10^8 cm⁻³
			$3p \rightarrow 4s$	$3p \rightarrow 4p$	$3p \rightarrow 4d \rightarrow 4p$	$3p \rightarrow 3d \rightarrow 4p$	4p	4s	4p	4s	4p	4s	
0.21	160	$T_e=5.6$, $N_e=2.9$	1.7	2.4	0.14	0.02	2.6	4.3	2.0	0.12	1.1	0.2	0.9
	330	$T_e=9.2$, $N_e=2.9$	7	10.8	0.91	0.06	11.8	18.8	8.3	0.66	4.6	1.1	3.5
0.37	160	$T_e=5.2$, $N_e=5.4$	5.2	5.8	0.36	0.29	6.5	11 7	4.7	0.42	2.6	0.7	1 9
	330	$T_e=9.0$, $N_e=5.2$	23	31.6	2.7	0.90	35.2	58.2	25.6	2.0	14.2	3.3	10.9
0.62	160	$T_e=3.2$, $N_e=14.4$	4.6	4.0	0.10	3.06	7.1	11.8	2.9	1.6	1.6	2.6	−1.0
	330	$T_e=6.5$, $N_e=13$	61	99.6	6.2	35	141	202	80.3	15.4	44.6	25.6	19.0

values of $\langle v_e\sigma_e \rangle$ given in Table VII. As seen from Table VIII, in all the regimes the pumping rates in the 4s and 4p configuration from the ground state are practically the same and lie in the range from 10^{17} to 10^{19} cm^{-3} sec^{-1}. The rate of pumping due to the 3p → 4d → 4p cascade process amounts to not more than 9% of the pumping into the configuration 4p from the ground state. It is listed in the fifth column and was calculated in accordance with the expression $0.060\ N_e^2 \langle v_e\sigma_e \rangle_{3p \rightarrow 4d}$, where the coefficient 0.060 is equal to the ratio of the radiative probability of the 4d → 4p transition (2.3×10^8 sec^{-1}) to the sum of the probabilities of the transitions 4d → 4p and 4d → 3p (see Fig. 26). The rate of pumping into the 4p configuration as a result of the 3p → 3d → 4p stepwise process was calculated by starting from the population of the configuration 3d, and determined by pumping from the ground state and by radiative decay, with allowance for the dragging of the radiation, which leads to an increase of the lifetime of the level. According to the theory developed in the papers of L. M. Biberman[108] and T. Holstein[109], for a cylindrical volume of radius R and an optically thick layer, the radiative rate of deactivation of the level decreases by a factor g^{-1} in comparison with the natural rate, with

$$g = 1.60/K_0R\,[\pi \ln (K_0R)]^{1/2}, \qquad (16)$$

where K_0 is the absorption coefficient at the center of the Doppler-broadened line. Calculation by means of this formula have shown that at an argon-ion concentration on the order of 10^{14} cm^{-3} the lifetime of the 3d configuration increases by 14–18 times, a fact accounted for in Table VIII.

Knowing the population of the 3d configuration, it is possible to determine the 3d → 4p pumping rate. It is equal to $N_{3d} N_e \langle v_e\sigma_e \rangle_{3d \rightarrow 4p}$. As seen from the sixth column of Table VIII, the contribution made to the pumping to the 4p configuration by process 3p → 3d → 4p does not exceed 5% of the pumping from the ground state at pressures $p_0 = 0.21$–0.37 Torr, and becomes comparable with the pumping from the ground state at $p_0 = 0.6$ Torr. The contribution due to the radiative cascades from configurations 5s, 6s, ... and 5d, 6d, ... was not taken into account in Table VIII, since the value of $\langle v_e\sigma_e \rangle$ for the population of these configurations from the ground state is much smaller than for the processes considered above.

Table VIII gives also the total rates of pumping into the configurations 4p and 4s and their populations. The rate of pumping to the 4s configuration is always higher than to the 4p configuration. This is natural, since radiative cascades from the 4p configuration goes to the 4s configuration in addition to the electron pumping from the 3p configuration. In calculation the population of the 4s configuration, just as in the case of the 3d configuration, account was taken of the dragging of the radiation, which becomes appreciable when $N_e > 10^{14}$ cm^{-3}.

In calculating the population of the 4p configuration, besides the radiation 4p → 4s transition, account was taken of the electron deactivation of this configuration as a result of the transitions 4p → 3d and 4p → 4s. At electron concentrations on the order of 10^{14} cm^{-3}, up to 28% of the transitions were due to collisions with electrons. Thus, an electron concentration on the order of 10^{14} cm^{-3} is critical. At this concentration, destruction of the inversion begins as a result of electron collisions and dragging of the radiation.

Returning to Table VIII, we see that in spite of the fact that the rate of pumping into the 4s configuration is always higher than into the 4p configuration, its population is always lower than that of 4p, in view of the much higher rate of radiative decay of the first configuration compared with the second. This occurs

even when a decrease occurs in the rate of radiative decay as a result of dragging of the radiation. It is also seen from the table that the population of the configuration 4p reaches almost 10^{11} cm^{-3}.

An important factor, in estimating the degree of activity of a laser medium from its gain is, of course, not the population of the configurations of the levels, but the populations per unit statistical weight (USW). Before we consider these data, we should make two remarks. First, in connection with the fact that the degree of deviation of the excitation of the states of the configurations of Ar II from the LS coupling is small[37], the values of $\langle v_e\sigma_e \rangle$ and the pumping rates given in Table VII pertain to the doublet system of terms. In the LS-coupling approximation, the quartet system of levels will be populated much less intensely, and only as a result of exchange interaction. Thus, we have every reason for assuming that the data listed in Table VII pertain to the doublet system of terms*. Second, to estimate the populations of the levels of configurations 4s and 4p per unit statistical weight we must know how the populations listed in the table will be distributed among the levels of these configurations. In view of the lack of these data, we make the most natural assumption that the distribution of the populations among the levels within the configurations is proportional to the statistical weights. Under these two assumptions, the populations and the inversion per unit statistical weight were calculated for the 4s and 4p configurations (the statistical rate of the doublet system of the terms of the 4s configuration is 6, and for the 4p configuration it is equal to 18).

We shall now discuss the results listed in the table and compare them with experiment. As seen from the table, the electron temperature increases with increasing current density at all pressures, leading to an increase in the pumping rate and in the inversion density. In Table IX are given the experimental data on the population of the 4p configuration as obtained from three published papers[87,110,111]. The measurements were made in a discharge tube of 2 mm diameter. Data on the level populations of the 4p configuration were obtained from measurements of the absolute intensities of the lines that begin from the levels of this configuration. The theoretical values of the populations were obtained by linear interpolation between the data of Table VIII.

Table IX. Populations of 4p (and 4s) configuration

Discharge parameters		Population per USW		Reference
p_0, Torr	j, A/cm^2	Experiment	Theory	
0.2	220	$(2.5-2.7)\cdot10^8$	$2.5\cdot10^8$	111
0.67	160	$(2-3)\cdot10^8$	$1.3\cdot10^8$	87
0.3	160	$(4-8)\cdot10^8$	$3\cdot10^8$	110
		$5\cdot10^8$ (4s)	$0.7\cdot10^8$ (4s)	110

*According to estimates, the electronic cross section for the excitation of quartet levels from the ground state of Ar II are smaller by a factor of 5 – 10 than for the doublet levels.

Table X gives a comparison of the calculated values and of the experimental values (measured in[110,114] as well as at FIAN) of the inversion between the $4p^2D_{5/2}$ and $4s^2P_{3/2}$ levels. As seen from Tables IX and X, the agreement between the calculated and experimental values is satisfactory if account is taken of the very crude assumption that the distribution of the population among the levels of the configuration is proportional to the atomic statistical weights, of the inevitable experimental errors*, and of the somewhat different experimental conditions. More reliable calculations can be made only after calculating the values of $\langle v_e\sigma_e \rangle$ for the levels. We now compare the attainable pumping rates (according to the calculations) with the experimentally observed output powers. The highest specific power attained with an Ar^+ laser of continuous action (without a magnetic field) is 1 W/cm^3. Such an output power requires a pumping rate of 2×10^{18} cm^3/sec. It is seen from Table VIII that at an optimal pressure 0.37 Torr) and at $j = 330$ A/cm^2, the calculated pumping rate even exceeds that necessary to obtain the highest powers, Thus, at the plasma parameters used by us, the considered processes pump the working levels of the Ar^+ laser with an adequate margin. The situation is different if we assume, in accordance with[83,87], a plasma temperature ~20,000°K. In this case $\langle v_e\sigma_e \rangle$ for the $3p \rightarrow 4p$ transition is equal to 4.7×10^{-13} cm^3/sec. At this value of $\langle v_e\sigma_e \rangle_{3p\rightarrow4p}$, to ensure the pumping rates 10^{18} cm^3/sec necessary to obtain specific generation powers of 1W/cm^3, the charged-particle concentrations must exceed 10^{15} cm^{-3}, i.e., much higher than the limiting concentration at which the population inversion is destroyed both as a result of electron collisions and as a result of dragging of the radiation. It therefore follows inevitably that the electron temperature of the Ar^+ laser plasma exceeds 20,000°K. Summarizing the results of the experiments and the calculations, it should be noted that the discussed mechanism of the Ar^+ laser operation apparently describes the situation correctly. The main process of pumping to the upper laser configuration is the electronic process of the population from the ground state of the ion, namely $3p \rightarrow 4p$ with addition of the cascade excitation $3p \rightarrow 4d \rightarrow 4p$ and the stepwise excitation $3p \rightarrow 3d \rightarrow 4p$. The main process ensuring deactivation of the lower laser configuration is the radiative transition $4s \rightarrow 3p$.

We note that the further development and refinement of the mechanism of inversion production in Ar^+ lasers are connected primarily with calculations of the electron cross sections for the excitation of individual levels. One can expect the roles of the cascades and of the stepwise excitation to increase for the individual transitions. This pertains first of all to the $4p^2D_{5/2} \rightarrow 4s^2P_{3/2}$ transition (λ 4880 Å), which makes the maximum contribution to the generation, since the largest part of the radiative transitions from the con-

*In addition to populations of the levels of the 4p configuration, R. Rudko and S. Tang [110] determined, from the gain, the population per unit atomic weight of the levels of the 4s configurations. It turned out to be equal to 5×10^8 cm^{-3} and differed greatly from the theoretical value 0.5×10^8. One cannot exclude the possibility that this discrepancy is connected with an experimental error.

Table X. Inversion per USW, 10^8 cm^{-3}.

p_0, Torr	$j = 180$ A/cm^2			$j = 200$ A/cm^2			$j = 270$ A/cm^2		
	Calculation	Experiment		Calculation	Experiment		Calculation	Experiment	
		⌀ 2.8 mm (FIAN)	⌀ 2.0 mm 110		⌀ 2.8 mm (FIAN)	⌀ 2.5 mm 111		⌀ 2.8 mm (FIAN)	⌀ 2.5 mm 111
0.2	0.75	1.5	—	1.6	2.7	—	2.6	5.1	—
0.3	1.35	2.2	2.5	2.6	3.7	6.3	4.5	6.3	9.8
1.0	—	—	—	—	0.9	—	—	4.3	—

figuration 4d goes to this level, just as the largest part of the transitions from the metastable level $3d^2F_{7/2}$ also goes to this level. Special attention must be paid to the clarification of the role of the metastable levels in the population of the laser levels. It is possible that this may be precisely the reason why the calculated values of the population inversion are systematically lower than the experimental ones (see Tables IX and X).

So far we have discussed the operating mechanism of the Ar^+ laser without a magnetic field. In view of the lack of reliable data on the parameters of the plasma in the magnetic field, the influence of the magnetic field on the operation of the laser will be discussed only qualitatively, using as an example a discharge in a capillary of 2.8 mm diameter at $p_0 = 0.37$ Torr and $j = 160$ A/sec^2. As is seen from Table VI, when the magnetic field increases from 0 to 700 G, the electron temperature decreases from 52,000 to 33,000°K, which leads, in accordance with interpolation of the data of Table VII, to a decrease in the pumping rate by an approximate factor of 10. Experiment shows that in spite of the decreased excitation rate, the intensity of the spontaneous emission of the Ar II lines doubles when the magnetic field increases from 0 to 700 G. This means that N_e should increase at least by a factor of 4.5 (account must be taken of the quadratic dependence of the pumping rate on the concentration of the charged particles).

It is not excluded that an appreciable role in the growth of the intensity of the spontaneous emission (and also in the stimulated emission) of the Ar II lines is played by the change in the distribution of the charged particles over the cross section of the discharge. It is obvious that narrowing of the distribution curve of the charged particles leads to an increase in the pumping rate in the near-axial sections of the discharge, which contribute most to the generation. If we accept the hypothesis, which is confirmed by[97,112,113], that the temperature decreases and the charged-particle concentration increases with increasing intensity, then the existence of a magnetic field that is optimal from the point of view of the generation power becomes understandable.

In fact, the increase of the magnetic field plays a favorable role in the pumping only so long as the associated decrease of the electron temperature, which leads to a sharp decrease of the pumping rate $\langle v_e\sigma_e \rangle$, is more than offset by the increase of the electron density on the discharge axis. At a sufficiently high magnetic field intensity, obviously, there will be no such compensation and then the magnetic field will play an unfavorable role. An important role in the existence of the optimal magnetic field is apprently played also by the dragging of the radiation, the importance of which increases with increasing magnetic field, since the concentration of the charged particles increases. The major role played by the dragging of the radiation in the existence of an optimal magnetic field is evidenced by the experiments of Gorog and Spong[42]. The decrease of the generation power in magnetic fields larger than optimal can hardly be attributed to the occurrence of instabilities and the resultant increase of the interaction between the discharge and the walls. If this effect were to play any role, then an appreciable growth of the longitudinal electric field intensity would be observed with increasing magnetic field; this did not occur.

The foregoing demonstrates the unsatisfactory situation in the understanding of the operation of the Ar^+ laser in a magnetic field, and the need for organizing experiments aimed in particular at clarifying the influence of the magnetic field on the temperature and concentration of the electrons and of their radial distribution.

VIII. FREQUENCY SPECTRA OF LONGITUDINAL MODES IN AN ARGON ION LASER

The first to investigate the frequency spectrum of the longitudinal modes of Ar^+ lasers were W. Rigrod and T. Bridges[115] at λ 4880 Å. They used a scanning Fabry-Perot interferometer 2.5 cm thick with a resolution limit of 30 MHz. They investigated the fundamental transverse mode TEM_{00}, while the higher modes were suppressed by means of a diaphragm. It was observed that a generation spectrum with stable amplitudes is obtained only near the threshold of the line excitation. A characteristic feature of this spectrum is the increased interval between the generation frequencies, amounting to several frequency intervals of the resonator c/2L (L—resonator length, c—speed of light). When the discharge current increases above a certain critical value, the character of the generation changes abruptly, and generation of unstable amplitude sets in at all the resonant frequencies. Distinct maxima were observed in the envelope of the amplitudes of the unstable-generation spectrum.

Figure 27 shows time-scan photographs of the unstable-generation duration in the longitudinal modes ranges from 1 to 5 μsec. It decreases with increasing discharge current and with increasing resonator Q. The total generation power at all frequencies remains constant in time, and all that occurs is a redistribution of the power among the oscillations modes. The distance between the simultaneous degenerated frequen-

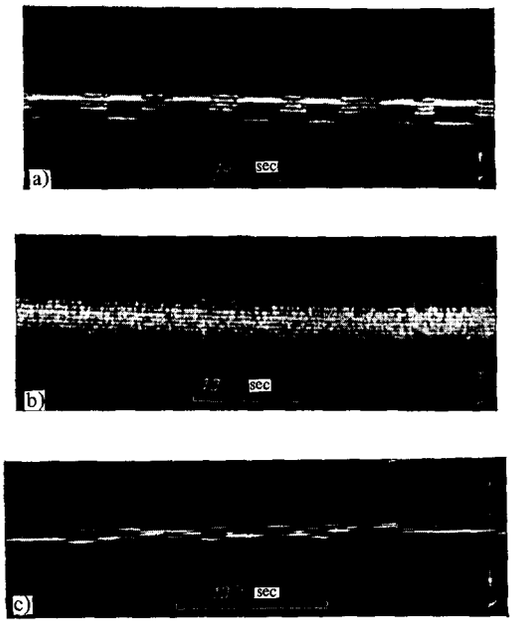

FIG. 27. Spectrum of longitudinal modes with a time sweep, in the case of 4880 Å generation of an Ar^+ laser without a magnetic field (TEM_{00} mode) [116]. a) Transition from stable generation at two frequencies to unstable generation of the residual pulsations of the rectified current; discharge current i = 4 A. b) Unstable generation at a current i = 10 A. c) Section of the spectrum near the center of the line at a large sweep rate: i = 10 A. The length of the laser capillary is 23 cm, the inside diameter is 2 mm, the pressure is p_0 = 0.3 Torr, the resonator length is L = 1 m, the thickness of the Fabry-Perot interferometer is 2 cm.

cies amounts, as a rule, to several times c/2L. In all other respects, the spectrum fluctuations have a random character. An analogous picture of frequency fluctuation was observed at λ 5145 Å. The total width of the generation spectrum at λ 4880 Å, at a current of 10 A, reached 9 GHz. The much larger spectral width, compared with the He-Ne laser, is attributed to the broader Doppler line and to the higher excess gain (excess of gain over resonator loss).

The characteristic features of the frequency spectrum of the Ar^+ laser, namely the spreading of the f spectrum in the near-threshold region and the unstable generation at higher excitation levels, are determined by the competition between the longitudinal modes. This competition occurs because at the customary employed resonator lengths the widths of the dips produced in the amplification contour by the individual modes exceeds the intermode resonator interval c/2L, owing to the large Lorentz line width $\Delta\nu_L$ of the working transitions, which, according to[81], amounts to 500 MHz. For this reason, in particular, the interval between the frequencies of the stable generation in the region of the threshold currents does not depend on the length of the resonator and corresponds approximately to the quantity $\Delta\nu_L$[116]. Both the spreading of the spectrum and the unstable generation are observed also in He-Ne lasers on λ 6328 Å, but there they occur only at large resonator lengths[116-118]. This difference is due to the smaller Lorentz width of the Ne line[119].

The described results were obtained with an Ar^+ laser without a magnetic field. Superposition of an external magnetic field, as shown in[120], shifts the limit of unstable generation towards larger discharge current. In[121], in the present of the magnetic field of 425 Oe, a stable two-mode spectrum at λ 4880 Å is observed up to a radiation density 11 W/cm² inside the resonator* (Fig. 28). The frequency interval between the modes, equal to cn/2L, where n is an integer, increases with increasing power, and furthermore in such a way that n is linearly dependent on the amplitude of the electric field in the resonator. The authors assume that as a result of the nonlinear interaction in the amplifying medium, the generated modes are "linked" in phase. In this case, the output laser signal constitutes a sequence of sinusoidal beats with a repetition period T = 2L/nc. The experimentally determined amplitude of the pulses inside the resonator turn out to be much smaller than the amplitude of the "π pulses"† , determined from the relation

$$E\mu_{12}\tau/\hbar = \pi; \qquad (17)$$

Here E is the (average) amplitude of the field in the pulse, τ is the pulse duration, and μ_{12} is the matrix element of the dipole moment of the transition (it was assumed in the calculation that τ = T/2).

The foregoing experimental results agree qualitatively with the theoretical calculations of the mode-locking regime at a high excitation level[122]. This calculations shows that with increasing excitation level there should occur an increase of the pulse repetition frequency (an increase of n). The amplitudes of the pulses also increases, but no "π pulses" are realized in the presence of relaxation of the medium. We note that neglect of relaxation of the medium within the Ar^+ laser pulse time τ is in general impossible, owing to the very small lifetime of the lower working levels (see Ch. VI). Indeed, the minimum value of τ is connected with the bandwidth $\Delta\nu_g$ of the excess gain by the relation $\tau_{min} = 1/\Delta\nu_g$. Assuming $\Delta\nu_g \sim 10^4$ MHz[116], we obtain $\tau_{min} \sim 10^{-10}$ sec, which is comparable with the lifetime of the lower levels. It is interesting to note that in an He-Ne laser (λ 6328 Å), the self-locking regime is satisfactorily described by the theory of "π pulses," owing to the much lower relaxation rates of the working levels in this type of laser[118].

The shortest pulses, obtained in[121] at a radiation density ~11 W/cm² inside the resonator, had a duration ~0.5 nsec. Further increase of the power, insofar as can be judged from the mode-beat spectra given in[121], led to the appearance of unstable generation. At a radiation density 15 W/cm², the previously sharp peaks of the mode beats became strongly broadened. Their width reached ~500 kHz, in qualitative agreement with the frequency of the amplitude fluctuations of the unstable-generation modes observed in[116].

Direct observation of periodic pulsations in the

*By radiation density inside the resonator we mean henceforth the sum of the powers of the forward and backward waves per unit cross section of the beam.

†Pulses which would lead, in the absence of relaxation of the medium, to a change of the sign of the inversion of the working levels.

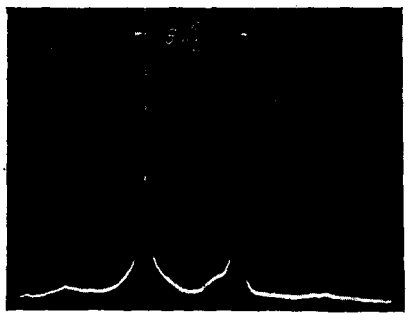

FIG. 28. Stable two-mode spectrum of Ar^+ laser at λ 4880 Å [121]. Capillary of diameter 3 mm and length 25 cm, current i = 30 A, H = 425 Oe. Resonator length L = 180 cm, internal radiation density I = 8 W/cm².

FIG. 29. Puslation in output radiation of an Ar^+ laser [123a]. 4880 Å line, resonator length L = 63 cm, capillary diameter 2.5 mm and length 2.5 cm, current 6 A, magnetic field H = 500 Oe. The frequency scale on the abscissa axis 2 nsec/div.

output signal of an Ar^+ laser, with repetition frequencies c/2L and 2c/2L was reported in[123a] and serves as direct proof of the feasibility of mode locking in this type of laser. The width of the pulses was 0.5 nsec at a repetition period of 4.2 nsec (Fig. 29). It can therefore be concluded that several longitudinal modes took part in the synchronization.

It is natural to propose that the stable generation spectrum observed in[115,116,120] at moderate excitation levels is the result of mode locking. When the excitation level increases above a certain critical value, the locking gives way to the free-generation regime, in which the amplitude and phases of the modes fluctuated randomly. The theory of the self-locking regime, developed in[118] as applied to He-Ne lasers, predicts that at sufficiently high excitation levels continuous generation of modes that are not coupled in phase ensures a more effective utilization of the inversion of the medium and accordingly gives a larger average generation power than the self-locking regime. Under these conditions, self-locking cannot be stable and gives way to continuous generation. Apparently, the same should be expected also in Ar^+ lasers. The broadening of the region of stable generation in a laser with a magnetic field may be connected both with the enhancement of the interaction of the mode as a result of the growth of the homogeneous line width, and with the general broadening of the line contour.

For an experimental verification of this assumption, it is necessary to investigate simultaneously both the mode spectrum of the laser and the pulsations of its output signal. Unfortunately, such investigations have not been performed as yet for Ar^+ lasers. The behavior of a stable two-mode spectrum at λ 4880 and 5145 Å with changing magnetic field intensity, up to H = 3500 Oe, was investigated in[123b]. It was found that the interval between the modes increases with increasing field, and, starting with H ~ 1000 Oe, it corresponds to the value of the Zeeman splitting of the σ components.

In concluding this chapter, we note that the fluctuations of the frequency spectrum of unstable generation may be a serious additional source of noise in the emission of multimode Ar^+ lasers.

IX. SINGLE-FREQUENCY LASERS

In many applications of argon ion lasers, for example in communication systems, holography, physical investigations of the scattering of light, and others, it is desirable to have single-frequency lasers capable of generating a single longitudinal mode.*

The axial-mode selection methods developed for He-Ne lasers, are in the main suitable also for Ar^+ lasers. However, owing to the appreciable amplification line width in the Ar^+ laser, additional difficulties arise in the mode selection. For this reason, in particular, no use is made of the method of simply shortening the resonator length[126]. On the other hand, the large Lorentz line width is favorable to mode selection. We shall consider below different methods of realizing a single-frequency regime in an Ar^+ laser.

The first report of successful single-frequency generation in Ar^+ lasers was that of P. Zory[127]. He used as the selecting element an additional resonator with a large separation of the natural frequencies, in accordance with a scheme previously used by P. Smith for He-Ne lasers[129]. Zory's setup is shown in Fig. 30. The additional resonator was made up of flat mirrors M_1, M_2, M_3, with M_1 and M_2 having a high reflection coefficient, while M_2, for which the coupling with the main resonator was effective, was semitransparent. The output mirror M_4, with a radius of curvature 2 meters, had a transmission of 9% for λ 4880 and 5145 Å. The optical path between the mirrors M_1 and M_2 was 2.12 cm. The length of the main resonator M_1,

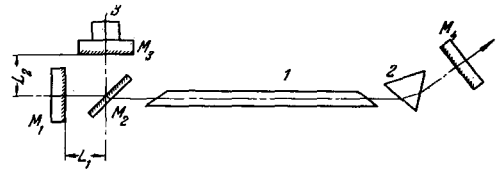

FIG. 30. Diagram of single-frequency Ar^+ laser with additional resonator [127]. 1 – Discharge tube, 2 – prism, 3 – piezoceramic block, M_1, M_2, M_3, M_4 – resonator mirrors.

*We shall not touch upon the question of the selection of the wavelengths corresponding to different Ar II transitions. This selection is attained best by placing a dispersive prism in the resonator [124]. Devices have also been developed, which make it possible to "switch over" rapidly to the generation wavelength [125]. Nor will we deal with the selection of transverse modes.

M_4 was 1 meter. The mirror M_3 was mounted on a piezoceramic block, which made it possible to tune the working frequency of the laser to the central part of the amplification line. To separate the wavelength of the working transition, a prism was placed in the resonator. A tube was used with a quartz capillary having an inside diameter 2 mm and a length 15 cm. The discharge current was 15 A at a pressure 0.5 Torr.

The action of Smith's three-mirror resonator is equivalent to the action of a mirror with a complex amplitude reflection coefficient[129]

$$r_e = \frac{t_2^2 r_1 \exp(-i\Phi_1)}{1 - r_2^2 r_1 r_3 \exp(-i\Phi)}, \quad (18)$$

where r_1, r_2, and r_3 are the reflection coefficients of the mirrors M_1, M_2, and M_3, t_2 is the transmission of the mirror M_2 (maximum values), $\Phi_1 = 4\pi L_1/\lambda$, $\Phi = 4\pi(L_1 + L_2)/\lambda$ (see Fig. 30). An analysis of (18) shows that the maxima of the reflection of the Smith resonator are analogous in shape and width to the maxima of the reflection of the plates $R_{FP} = R_2$ and the internal absorption, which are characterized by a transparency $\tau_{FP} = \sqrt{R_1 R_3}$ (R_1, R_2, and R_3 are the power reflection coefficients of the mirrors). The distance between successive maxima on the frequency scale is $\Delta\nu = c/2(L_1 + L_2)$, and the width of the maxima (at half-power level) amounts to

$$\delta\nu = \Delta\nu (1 - \sqrt{R_1 R_3} R_2)/\pi \sqrt{R_2 \sqrt{R_1 R_3}}. \quad (19)$$

The large width of the region of excess gain of the lines in Ar^+ lasers leads to the need for using additional resonators with an increased separation of the natural frequencies, $\Delta\nu$, compared with the He-Ne laser, although this is not favorable from the point of view of mode selection. In the cited paper[127], it was assumed that $\Delta\nu = 7000$ MHz. As to the widths of the maxima, it apparently suffices for them not to exceed the width of the dip produced in the amplification line by the generated mode[128]. In Ar^+ lasers, the latter can reach 1000 MHz and more. Substituting in (19) $\delta\nu = 7000$ MHz, $R_2 = 0.6$, and $R_1 = R_3 = 1$, we get $\delta\nu = 1100$ MHz. An increase of the reflection coefficient of the splitting mirror increases the selecting ability of Smith's resonator. We note that in all cases of axial-mode selection it is essential to suppress the higher transverse mode.

A residual generation power of 130 mW at λ 4880 Å and 120 mW at λ 5145 A was reached in[127]. The loss introduced by the Smith resonator was 6%. In a two-mirror resonator with identical value of the loss, the output power through the mirror M_4, in the same lines, amounted to 250 and 140 mW. However, when the Smith resonator is replaced by a high-reflectivity mirror, the corresponding figures increase to 490 and 330 mW. We see therefore that an important role is played in the lowering of the power of the single-frequency generation, compared with the multi-frequency generation, not so much by the narrowing of the generation spectrum and the associated decrease of the effectiveness of utilization of the inversion of the medium, as by the introduction of additional losses resulting from making the resonator more complicated.

The question of the ratio of the powers of the single-particle and many-particle generation was investigated theoretically and experimentally[130-132]. It was shown that in the ideal case, i.e., without account taken of the losses introduced by the additional resonator, it is possible to use in the single-frequency regime 60—70% or more of the power that the medium is capable of delivering in the multifrequency regime. This question will be considered in greater detail in the next chapter.

The same method was used in[132] to obtain the output power, 0.52 W, at one frequency λ 4880 Å. The laser had a discharge tube with inside diameter 3 mm and length 46 cm, and operated with an external magnetic field of 1100 Oe. The indicated power was reached at a discharge current 35 A. The magnetic field did not introduce any appreciable complications in this method, for in the presence of Brewster windows the degree of ellipticity of the polarized laser radiation is very small[133]. Production of single-frequency power of 2 W by an Ar^+ laser was reported in[134a]. In[134b] it was proposed to use a confocal resonator with an inclined axis as the additional resonator.

A serious and still and unresolved problem in this type of laser is the stabilization of the tuning of the additional resonator relative to the contour of the amplication line. The compact dimensions of the additional resonator facilitate the use of methods of passive stabilization. Thus, for example, in[135], to increase the mechanical stiffness of the system, it was proposed to use as the additional resonator a quartz prism with reflecting coating deposited on its faces. A shortcoming of the prism is the need for its thermal stabilization. The temperature drift of the prism-resonator frequency, due to the dependence of the refractive index of the quartz on the temperature, amounts in accordance with the authors of[135] to approximately 4700 MHz per degree C. Allowance must also be made for the possibility of thermal self-focusing of the radiation inside the prism.

Another no less complicated problem is the stabilization of the length of the main resonator relative to the length of the additional resonator. This problem is in many respects common to single-frequency and multi-frequency lasers, but it should be borne in mind that in the described single-frequency laser scheme the fluctuation of the main resonator leads to a change not only of the frequency but also of the amplitude of the output signal[129]. The indicated feature of the single-frequancy laser can be used to produce an error signal in the automatic frequency control system that regulates the length of the main resonator. Such a system was realized so far only for a single-frequency He-Ne laser[129].

L. Osterink and R. Targ[136] used a method of separating monochromatic radiation from frequency modulated (FM) spectrum of an Ar^+ laser. This method was earlier used in He-Ne lasers[137]. A schematic diagram of the method is shown in Fig. 31. The depth of modulation of the phase Γ in the FM signal of the laser is determined by the relation[138]

$$\Gamma = (\delta/\pi)(\Delta\Omega/\Delta\omega), \quad (20)$$

wgere $\Delta\omega = \omega_m - \Delta\Omega$ is the deviation of the modulation frequency ω_m relative to the distance between the

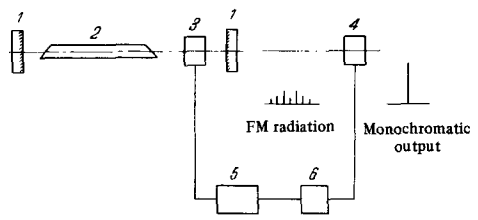

FIG. 31. Diagram of single-frequency Ar^+ laser with frequency modulation [139]. 1 – Resonator mirrors, 2 – discharge tube, 3 – internal phase modulator, 4 – external phase modulator, 5 – high-frequency generator, 6 – phase shifter.

modes $\Delta\Omega$, and the value of δ is approximately equal to the maximum delay of the phase per pass in the internal modulator (the customarily employed values of δ lie in the range 0.01–0.2 rad). A similar depth of modulation of the phase Γ should be obtained also by means of an external modulator, which demodulates the FM spectrum into a monochromatic signal.

Given ω_m, the value of Γ determines the width of the spectrum of the FM signal. In order to obtain in the output radiation of the signal a single FM signal and to suppress all others, this width should be chosen so as to correspond approximately to the width of the region of the excess gain of the line. It is clear therefore that in the Ar^+ laser, with the broad Doppler line and relatively high gain, it is necessary to have much higher Γ than in He-Ne lasers. According to[136], the required values of Γ for λ 5145 Å lie in the range 3.8–4.7 rad in the region of output powers 250–400 mW. For λ 4880 Å with the higher excess gain, the required value is $\Gamma = 10$ even at a power of 250 mW. (For comparison we indicate that $\Gamma = 2$ was used in[137] for an He-Ne laser). This circumstance creates difficulties in two ways. On the one hand, it is a rather complicated technical problem to ensure large phase shifts in the internal modulator. On the other hand, at large values of Γ there is danger of phase distortion of the FM signal[139]. The authors of[136] have therefore concluded that the use of this method is not advisable for λ 4880 Å and confined themselves to obtaining and investigating a signal-frequency output at λ 5145 Å.

Osterink and Targ[136] used in their setup a ring laser excited by a high-frequency discharge with active length 60 cm. The internal modulator was a KDP crystal. The modulation frequency 384 MHz corresponded to three times the intermode interval of the resonator. Thus, each third mode was coupled in the FM signal. The demodulation was by passing the beam twice through a lithium-niobate crystal 2 cm long. The depth of modulation $\Gamma = 4.5$ in the external modulator was attained at a modulating HF signal power of 2 W. The power of the monochromatic radiation at λ 5145 Å reached 350 mW. The power in the side bands did not exceed 0.1% of this value*.

The power of multi-frequency generation in the same line, in the absence of an internal modulator, was 800 W. The light loss in the external modulator was 11%. Theoretically, this method makes it possible to obtain 100% conversion of the laser power into a monochromatic output signal. In practice, however, the losses introduced into the resonator by the modulation cell lead to an appreciable lowering of the single-frequency power.

One of the advantages of the foregoing method is the possibility of stabilizing the FM signal frequency relative to the center of the Doppler line. To generate the error signal it is possible to use in the automatic frequency control system beats produced in the first side bands when the carrier of the FM signal deviates from the center of the line[140,141]. In this manner we obtained in[141] a long duration relative stability of He-Ne and Ar^+ laser frequencies amounting to 10^{-8}.

Worthy of attention is the method proposed by Yu. V. Troitskiĭ and N. D. Goldina[142] for selecting longitudinal modes with the aid of a thin absorbing film placed in the laser resonator. They used nickel films deposited on a quartz substrate; the films had an absorption coefficient 0.14 (in the traveling wave). When the film position coincided with the nodal surface of the electric field of the standing wave of one of the oscillation modes, the losses introduced by it in the given mode were very small (0.2–0.3% per pass). At the same time, for the other modes, the attenuation can be appreciable and these modes are suppressed. Thus, single-frequency generation was obtained in both He-Ne and Ar^+ lasers. A scattering film can be used in place of an absorbing film[142].

An interesting possibility of realizing single-frequency generation in an Ar^+ laser at λ 5145 Å was pointed out by J. Forsyth[143]. He used a resonator of a special type, in which the beams corresponding to λ 4880 and 5145 Å were separated on leaving the discharge tube with the aid of prisms, and each of the beams was directed to a separate mirror. When the optical lengths were equal for both beams, the spectra of each of lines revealed a typical picture of unstable generation. However, when the optical length of one of the beams was slightly changed, the character of the spectra also changed. Stable generation at two widely spaced modes appeared at λ 4880 Å, whereas single-particle generation took place at λ 5145 Å. The effect was observed in the magnetic-field intensity range 600–750 Oe. The power of the single-frequency output at λ 5145 Å was 70 mW.

There is no doubt that the observed phenomenon is based on the competition between transitions that are coupled through a common lower state. It can be proposed that the resultant two-mode regime at λ 4880 Å is analogous to that observed in the previously cited investigation[141]. For λ 5145 Å, which has a weaker gain, a regime of this type turns out to be "inconvenient" if the lengths of the optical paths are not equal, since it would be accompanied by a "superposition" of the pulses in the medium, owing to their different repetition frequencies for both lines. Under these conditions λ 5145 Å "prefers" degenerate at one frequency. (It should experience at the same time a weak amplitude modulation with a pulse repetition frequency λ 4880 Å.) Apparently, this is the way of finding the answer to the question why the difference in the optical lengths of the beams causes the random generation to give way to stable spectra*.

*The sidebands are due to amplitude and phase distortions of the FM signal or to its incomplete demodulation.

*For a quantitative interpretation of this phenomenon see [160].

In conclusion we note that most methods of realizing single-frequency Ar^+ lasers considered here are represented by single papers, and thus, these methods are not yet fully verified. The limited experimental material available at present does not make it possible to compare with assurance the shortcomings and advantages of the proposed constructions of single-frequency Ar^+ lasers.

X. GENERATION POWER IN MULTIFREQUENCY AND SINGLE-FREQUENCY REGIMES

Just as in the case of other gas lasers, a rigorous analysis of the processes of generation in Ar^+ lasers calls for the solution of nonlinear equations describing the oscillations of the field in the presence of the active medium. However, the well known method of W. Lamb[144] cannot be used to calculate the operating regimes of the Ar^+ laser of practical interest since it yields results only in the region of small saturation of the medium, i.e., under conditions close to the threshold of excitation of the lines. Satisfactory agreement with experiment is obtained by calculating the powers of gas lasers on the basis of a more simplified, the so-called probabilistic method[130,145-150]. Without going into details of the method and its principal limitations, let us see the results it yields in the case of Ar^+ lasers.

In an Ar^+ laser with an external magnetic field, calculations of the generated power are greatly complicated by the Zeeman splitting of the lines, and none have been published so far. We therefore confine ourselves to the case of a laser without a magnetic field.

A specific feature of the Ar^+ laser is the drift motion of the particles which leads to a difference between the gains of the forward and backward waves in the resonator. Attempts to take into account the drift motion[130] will be discussed later, where it will be shown that its influence on the generation power is not very appreciable. In all the relations presented below, with the exception of (21) and (22), it is assumed that there is no drift and that the ion velocity distribution is Maxwellian (relations (21) and (22) do not depend on this assumption). We shall henceforth use the following basic assumptions:

1) The upper and lower states of the working transitions, designated a and b, can be characterized by total decay probabilities γ_a and γ_b, and by a transition probability γ_{ab} that does not depend on the field amplitude or on the velocities of the radiating particles.

2) The presence of generation does not influence the level pumping rates S_a and S_b, with the exception of pumping in the a → b channel.

The foregoing assumptions are satisfied under the condition that it is possible to neglect the influence of the generation on the discharge parameters and on the populations of other Ar II levels, with which the working stage can exchange energy. It is also assumed that in level-decay processes it is possible to neglect ion-ion and ion-atom collisions. On the basis of the mechanism considered above for the discharge in the Ar^+ laser, one can expect, in first approximation, that these conditions are realized. The competition of the transitions that simultaneously take part in the generation is not taken into account here.

Under the foregoing assumptions, the equations for the balance of populations of the levels a and b yield for the power P_V generated in all types of oscillations by a single volume of the medium

$$P_V = h\nu T^{-1}(\Delta N^0 - \Delta N), \tag{21}$$

where $T = [(g_a/g_b)(\gamma_a - \gamma_{ab}) + \gamma_b]/\gamma_a\gamma_b$, g_a and g_b are the statistical weights of the levels, $\Delta N^0 = n_a^0 - n_b^0(g_a/g_b)$ and $\Delta N = n_a - (g_a - g_b)n_b$ are the values of the level inversion in the absence and in the presence of generation, expressed in terms of the ion densities n_a and n_b. In an Ar^+ laser we have $\gamma_b \geq \gamma_a$ and with good approximation $T^{-1} \approx \gamma_a$.

The maximum power that the medium can deliver in the state of total saturation ($\Delta N = 0$) is

$$P_V^{max} = h\nu T^{-1}\Delta N^0. \tag{22}$$

For the strong transitions of the Ar^+ laser at λ 4880 and 5145 Å we have $n_a^0 \gg n_b^0$ and $\Delta N^0 \approx n_a^0$. Consequently the maximum per-unit power of generation of these lines (based on the number of quanta) is equal to the pumping rate of the upper levels $S_a = n_a^0\gamma_a$, and thus, the "quantum yield" of these working transitions can approach unity.

Expressing the initial inversion ΔN_0 in terms of the coefficient of unsaturated gain at the center of the line $k^0(\nu_0)$, we get

$$P_V^{max} = \frac{4\pi^{3/2}h\nu^3 p\Delta\nu_D T^{-1}k^0(\nu_0)}{\sqrt{\ln 2}c^2 A_{ab}}, \tag{23}$$

where $\Delta\nu_D$ is the Doppler line width, A_{ab} is the Einstein coefficient for spontaneous emission, and p is a correction that takes into account the influence of the Lorentz broadening of the line[147] ($p \approx 1 + 2\sqrt{\ln 2/\pi} \times (\Delta\nu_L/\Delta\nu_D) \approx 1 + 0.94\,(\Delta\nu_L/\Delta\nu_D)$).

Formula (23) can be used to calculate the maximum per unit generation power of the laser without a magnetic field, by measuring the unsaturated gain of the transition. Thus, for λ 4880 Å at a value $k^0(\nu_0) = 0.015\ cm^{-1}$, formula (23) yields $P_V^{max} = 0.4\ W/cm^2$ (we use the values $A_{ab} = 8.45\ sec^{-1}$, $\gamma_a = 1.15\ sec^{-1}$[110], $\Delta\nu_D = 3700$ MHz, and $\Delta\nu_L = 500$ MHz[81]).

According to (21) and (22), the specific power P_V can be represented in the form

$$P_V = \varkappa P_V^{max}, \tag{24}$$

where the quantity $\varkappa = (\Delta N^0 - \Delta N)/\Delta N^0$ characterizes the efficiency of utilizing the inversion of the medium[130]. Whereas P_V^{max} is determined exclusively by the parameters of the medium, $\varkappa$ is determined to a considerable degree by the Q of the resonator and by the character of the spectrum (single-frequency or multi-frequency), although it depends also on the ratio of the Lorentz Doppler width of the lines.

The total power P, generated by the beam, is equal to

$$P = \int P_V\, dV = \bar{P}_V\bar{V}, \tag{25}$$

where $\bar{V}$ is the effective volume of the radiation field in the active medium, and $\bar{P}_V$ is the generated power averaged over the volume. The determination of $\bar{P}_V$

and of $\overline{V}$ is a complicated problem in the case of real lasers, especially if it is borne in mind that at relatively small capillary diameters it is necessary to take into account both the inhomogeneity of the laser field and the inhomogeneity of the active medium. Calculation of $\overline{V}$ for the principal transverse mode TEM_{00} in a homogeneous medium has been carried out in[151,152]. It is assumed below that both the radiation field and the active medium are spatially homogeneous. The output power of the laser P_{out} can be expressed as follows:

$$P_{out} = \xi P, \tag{26}$$

where ξ depends only the parameters of the resonator, determining the ratio of the useful transmission and losses. If the losses at the ends of the active medium are characterized by effective reflection coefficients R_1 and R_2, and the losses in the medium itself are neglected, then we have, with good approximation

$$\xi \approx (t_1\sqrt{R_2} + t_2\sqrt{R_1})/(1-\sqrt{R_1R_2})(\sqrt{R_1}+\sqrt{R_2}), \tag{27}$$

where t_1 and t_2 are the useful transmissions from both ends of the laser. In resonators with high Q we have $\xi \approx (t_1 + t_2)/(2 - R_1 - R_2)$.

The efficiency of utilization of the inversion κ, and consequently also the generated power, depend strongly on whether the generation takes place at many frequencies (in the usual two-mirror resonator) or whether single-frequency generation is obtained by one of the methods described above*. Let us consider these cases separately.

1. Multi-frequency generation. Owing to the large Lorentz line width in Ar^+ lasers, a good approximation to reality is the assumption of homogeneous saturation of the inversion and of the amplification in the entire generation spectrum interval[145,149]. In the case of homogeneous saturation of the gain, the gain $k(\nu)$ is the same for the forward and backward waves, and equals

$$k(\nu) = -\ln\sqrt{R_1R_2}/l, \tag{28}$$

where l is the length of the active medium. The effectiveness of the use of inversion of the multi-frequency regime $\kappa^{(m)}$ can be expressed with good approximation by

$$\varkappa_{\xi}^{(m)} = 2\Phi(pX)/\sqrt{\pi}pX, \tag{29}$$

where $X = -k^0(\nu_0)l/\ln\sqrt{R_1R_2}$ is the degree of gain saturation, $\Phi(z) = (\sqrt{\pi/2})z\,\mathrm{erf}(\sqrt{\ln z}) - \ln z$ is a function introduced in[145], and

$$\mathrm{erf}\,y = (2/\sqrt{\pi})\int_0^t \exp(-t^2)dt -$$

is the error function. (Expression (29) is not suitable near the threshold of line excitation, $X \sim 1$.) As expected, $X\kappa^{(m)}$ increases with increasing degree of saturation, and tends to unity in the limit as $X \to \infty$

*An exception is the method in which the FM regime is used. If the distribution of the amplitude of FM spectrum duplicates in some manner the distribution of the amplitudes in the absence of modulation, then this case corresponds more closely to the multi-frequency generation with respect to the values of κ and p.

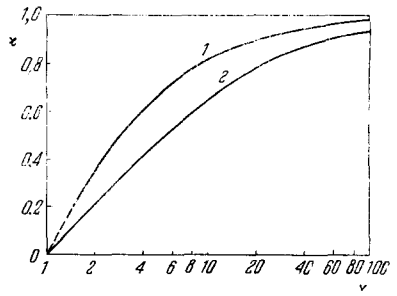

FIG. 32. Effectiveness of utilization of inversion $\kappa = P_V/P_V^{max}$ in the multi-frequency and single-frequency Ar^+ lasers, as a function of the degree of gain saturation X. 1 – Multi-frequency generation, 2 – single-frequency generation.

(Fig. 32). At a degree of saturation X = 10, which can be readily realized for strong transitions of Ar^+ lasers, the effectiveness of the utilization of inversion reaches 80%. From (23), (24), (26), and (29) we have for the output power

$$P_{out}^{(m)} = P_V^{max}\varkappa^{(m)}\xi V = \frac{8\pi h\nu^3}{c^2}\frac{\Delta\nu_D}{\sqrt{\ln 2}}\frac{T^{-1}}{A_{ab}}\Phi(pX)(-\ln\sqrt{R_1R_2})\xi S; \tag{30}$$

here V is the volume of the radiation field in the active medium and S is the cross section of the beam. In the case of low resonator losses $(-\ln\sqrt{R_1R_2})\xi \approx (t_1 + t_2)/2$. The radiation density I inside the resonator is connected with the per unit generated power by the relation $P_V = kI$, where k is given by (28). Therefore, taking (30) into account, we obtain for the internal radiation density in the multi-frequency regime

$$I^{(m)} = \frac{8\pi h\nu^3}{c^2}\frac{\Delta\nu_D}{\sqrt{\ln 2}}\frac{T^{-1}}{A_{ab}}\Phi(pX). \tag{31}$$

Comparison of (31) with experiment was carried out for Ar^+ lasers in[131,153,154]*. The degree of the saturation of the gain X was varied by placing in the resonator cavity a calibrated attenuator. It was found that the relation (31) agrees satisfactorily with the experimental data (Fig. 33). Figure 34 shows the experimental gain saturation curves at λ 5145, 4880, and 4765 Å[154]. The internal radiation density I, which leads to a decrease of the gain by a factor of 2(X = 2), amounts to 23, 160, and 30 W/cm^2 for the indicated lines, respectively.†

The slower saturation of the gain for λ 5145 Å is

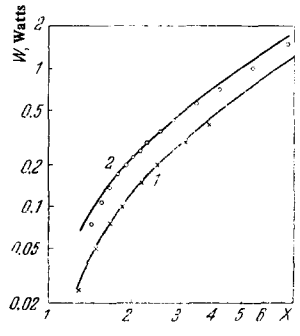

FIG. 33. Dependence of the internal power W = IS on the degree of gain saturation [131]. Current density j = 300 A/cm^2, p_0 = 0.3 Torr. 1 – Single-frequency regime, 2 – multi-frequency regime. The theoretical data (solid curves) have been normalized in such a way that at X = 2 there is exact agreement with the experimental data (O, X).

*The correction factor p was not taken into account in [153,154].

†The data presented have been refined by the authors of [154].

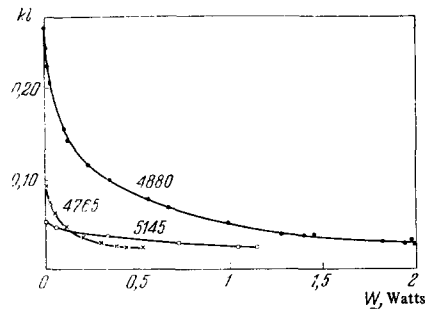

FIG. 34. Gain saturation curves for three Ar^+ laser lines as functions of the internal power W [154]. The current density is j = 300 A/cm², p_0 = 0.3 Torr, the capillary length is l = 23 cm, and the inside diameter is 2 mm.

connected with the fact that for the given transition the ratio $T^{-1}/A_{ab} \approx \gamma_a/A_{ab}$ is much higher than for the other two lines[37]. For this reason, λ 5145 Å which has a small gain, becomes comparable in power with λ 4880 Å at high excitation levels. The theoretical values of I and X = 2, calculated from (31) under the assumption that the rates of decay of the levels are determined by the radiative transitions and that $\gamma_{ab} = A_{ab}$, amount to 15.2, 187, and 20.4 W/cm² for λ 4880, 5145, and 4765 Å, respectively (we used for γ_a and γ_{ab} the values of[37], and for the decay probabilities of the lower levels we assumed $\gamma_b = 2.8 \times 10^9$ sec^{-1}[155]). These quantities are in satisfactory agreement with the experimental data presented above.

2. Single-frequency generation. In this case a dip is formed in the amplification contour, and its depth and shape depend on the degree of saturation X and on the position of the generation frequency ν relative to the center of the line ν_0. (At a large deviation $\nu - \nu_0$, two dips may be produced.) The generated power is easiest to calculate for $\nu = \nu_0$, although the power is not maximal in this case. According to[147], at $\nu = \nu_0$, the saturation of the gain as a function of the internal density of the radiation is given by the expression

$$(pX)^{-1} = (1+\mathcal{J})^{-1/2} \exp[(1+\mathcal{J}/\varepsilon^2)[1-\operatorname{erf}(\varepsilon\sqrt{1+\mathcal{J}})]; \quad (32)$$

here $\epsilon = \Delta\nu_L\sqrt{\ln 2}/\Delta\nu_D$, $\mathcal{J} = I/I_0 = 4\pi^2 h\nu^3 T^{-1}\Delta\nu_L/c^3 A_{ab}$ is the saturation parameter.

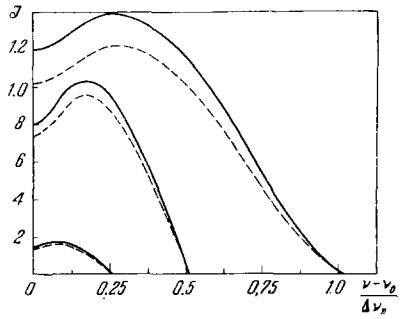

FIG. 35. Theoretical dependence of the internal radiation density $\mathcal{J} = I/I_0$ on the generation frequency deviation relative to the center of the Doppler line at different excitation levels. It is assumed that $\Delta\nu_L/\Delta\nu_D$ = 0.167 and the drift parameter is $\mathcal{D} = 0$ (solid curves) and $\mathcal{D} = 0.2$ dashed curves). The ordinate scale for the upper pair of curves is magnified ten times.

The effectiveness of utilization of inversion in the single-frequency regime, $\kappa^{(S)}(X)$, can be determined from the relation

$$\varkappa^{(S)}(X) = \varepsilon\sqrt{\pi}\,\mathcal{J}(X)/pX, \quad (33)$$

where $\mathcal{J}(X)$ is determined from (32). As seen from (33), $\kappa^{(S)}(X)$ depends strongly on the ratio of the Lorentz and Doppler line widths, increasing with decreasing $\Delta\nu_L/\Delta\nu_D$. As noted in Ch. V, in the Ar^+ laser the Doppler line width of the ions can vary noticeably, depending on the experimental conditions. Figure 32 shows the values of $\kappa^{(S)}$ calculated from (32) and (33) for the value $\Delta\nu_L/\Delta\nu_D = 0.135$, corresponding to $\Delta\nu_L$ = 500 MHz and $\Delta\nu_D$ = 3700 MHz "longitudinal" ion temperature is ~3000°K)*. The quantities $\kappa^{(S)}$ and $\kappa^{(m)}$, as follows from (24), are proportional to the powers generated by the medium in the single-frequency and multi-frequency regimes. It is seen from Fig. 32 that at sufficiently large X the indicated values of the power become close in magnitude. This is perfectly natural, since in the case of strong gain saturation in the Ar^+ laser, the homogeneous width of the radiation-broadened line, which equals $\Delta\nu_L\sqrt{1+\mathcal{J}}$ [128], becomes comparable with the width of the generation spectrum in the multi-frequency regime. This conclusion is confirmed by experimental comparison of the power of single-frequency and multi-frequency Ar^+ lasers[127,131,132] (see Fig. 33). For X = 2, the theoretical ratio of the single-frequency power (at zero detuning) to the multi-frequency power is 0.6. The experimental value of this ratio, in accordance with the data of[131], is 0.55. As to the output power of the single-frequency laser, as already noted, it can decrease additionally as a result of the losses inherent in the employed mode-selection methods (the losses lead to a decrease of ξ in formula (26)).

The dependence of the power on the frequency deviation $\nu - \nu_0$ was calculated with allowance for the drift in[130]. The following expression was obtained for the gain (averaged for the forward and backward waves):

$$k = \frac{\Delta N^0}{2}\frac{\sigma_0\gamma^2}{\sqrt{\pi}u}\int_{-\infty}^{+\infty}\frac{\exp\{-[(v-v')/u)]^2\}\,dv}{[L_+(\omega,v)+L_-(\omega,v)]^{-1}+\gamma^2\mathcal{J}}, \quad (34)$$

where the following notation was used: $L_\pm(\omega, v) = [\gamma^2 + (\omega_0 - \omega \pm Kv)^2]^{-1}$, $\sigma_0 = (\lambda^2/4\pi)(A_{ab}/\gamma)$, $\gamma = \pi\Delta\nu_L$, $K = 2\pi/\lambda$, $u = \sqrt{2kT/M}$, M ion mass, v'—drift velocity, and ω—circular frequency. With the aid of (34), the gain was calculated as a function of the parameters $\Delta\nu_L/\Delta\nu_D$, $(\nu - \nu_0)/\Delta\nu_D$, $\mathcal{J}$, and the drift parameter $\mathcal{D} = v'/u$. A computer was then used to determine the values of $\mathcal{J}(\nu - \nu_0)$ at a specified value of k and at fixed values of $\Delta\nu_L/\Delta\nu_D$ and $\mathcal{D}$. Figure 35 shows the theoretical curves of $\mathcal{J}[(\nu - \nu_0)/\Delta\nu_D]$ for two values of the drift parameter, while Fig. 36 shows a comparison of the calculated and experimental curves. In the theoretical curve on Fig. 36, the value of $\Delta\nu_L$ was chosen in such a way as to ensure the best agreement with the experimental curve, while the values of $\Delta\nu_D$ and $\mathcal{D}$ were taken from[81]. It is seen from the foregoing results that the depth of the Lamb hole in Ar^+ lasers can amount in typical cases to ap-

*In [132] they calculated the values of $\kappa^{(S)}(X)$ for $\Delta\nu_L/\Delta\nu_D$ = 0.24.

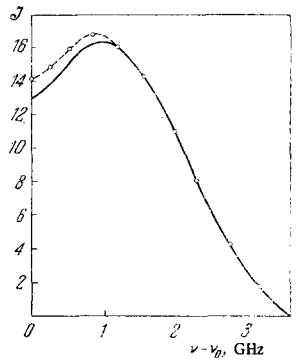

FIG. 36. Experimental plot of the internal radiation density J vs. the frequency deviation (dashed line) and theoretical curve of "best approximation." For the theoretical curve it is assumed that $\Delta\nu_L$ = 435 MHz and $\mathfrak{D}$ = 0.157.

proximately 20% of the maximum generation power. This is confirmed by the results of[131], where they measured experimentally the Lamb hole in the λ 4880 Å line. As follows from Fig. 35, the drift motion does not influence greatly the power, although it still leads to a certain decrease of the power. Attention is called to the noticeable discrepancy between the theory and experiment at frequencies near the center of the line. As noted in[130], it is connected with the approximate character of the probability method used in the calculations.

We shall not discuss the choice of the optimal resonator parameters, particularly the mirror transmission coefficients needed to obtain the maximum output power of the Ar^+ laser. Optimization of the mirror transition reduces to a determination of the maximum of the product $\xi\kappa$, which can be carried out with the aid of the relations and diagrams given above. In the case of the multi-frequency generation regime, one can use without appreciable error the results obtained without allowance for the Lorentz line width[146,148]. In single-frequency Ar^+ lasers it is necessary to take into account the Lorentz line width, as was done[159] for the He-Ne laser.

XI. CONCLUSION

In the four years elapsed since the construction of the first continuous Ar^+ laser, much progress was made both from the point of view of the development of different Ar^+ laser designs and from the point of view of clarifying the physical processes that ensure inverted population. At the present time, commercial Ar^+ lasers are produced with power up to 10 W and with service life up to 1000 hours. Under laboratory conditions, output powers up to 100 W were obtained in individual cases. However, the Ar^+ laser still remains an instrument difficult and expensive to construct, and this greatly hinders its application in scientific research and for practical purposes.

Recent theoretical and experimental investigations of the physical processes in the Ar^+-laser plasma have made it possible to understand the main features of the mechanism of inversion production in this type of laser. This makes it possible to approach more rationally the design and construction of lasers with optimal parameters and operating conditions. However, we still do not have a sufficiently complete picture with respect to the properties of the active medium of the Ar^+ laser, and many important problems still wait their solution. This pertains primarily to the role played by the magnetic field in the increase of the Ar^+ laser power, which is all the more important since the majority of Ar^+ lasers operate with a magnetic field. Nor is the mechanism of pumping the quadruplet terms of the 4p configurations completely clear, particularly, the role played in this pumping by the metastable 3d states. It is necessary to carry out theoretical and experimental investigations of the discharge parameters in sectionalized lasers and in lasers with radio-frequency supply. Of important practical value is the study of the processes that lead to the destruction of the internal walls of the tubes in Ar^+ lasers of various types.

To estimate the prospects of further increase in the Ar^+ laser power, great interest attaches to an investigation of the role of various factors that lead to the saturation of the generation power at high discharge-current densities.

Of fundamental significance for the Ar^+ laser is the problem of increasing its efficiency. The efficiency problem is particularly acute in the case of high-power lasers, since the present low efficiency lasers require power supplies on the order of dozens of kilowatts. Special investigations of the influence exerted on the efficiency by various factors (tube geometry, discharge conditions, etc.) and of the most economic methods of exciting Ar^+ lasers are needed. One of the promising ways of increasing the output power and efficiency of Ar^+ lasers is to use large-diameter discharge tubes.

Only the first, albeit important steps have been made in the investigation of the frequency characteristics of the Ar^+ laser emission and in the development of single-frequency lasers. Further research is needed on mode interaction in multi-frequency lasers and, in particular, on the conditions for the existence of mode-locking and the characteristics of this regime. As to the single-frequency lasers, it is desirable to have a better idea of the characteristics of different mode selection methods in Ar^+ lasers, and of the comparative advantages and shortcomings of such methods. One of the unsolved problems is the calculation of the power of multi-frequency or single-frequency Ar^+ lasers operating with a magnetic field.

The development of frequency-stabilized Ar^+ lasers is in a very unsatisfactory state. Although many of the frequency-stabilization methods proposed and realized for He-Ne lasers can apparently be used also in the case of Ar^+ lasers, there are practically no reports of work in this direction.

Foremost among the technical problems, as before, is the finding of discharge-tube materials and designs, capable of withstanding high current densities and ensuring at the same time the maximum service life, and also the development of methods of preventing splattering of the windows and mirrors of powerful Ar^+ lasers.

This, briefly, is a list of the main problems in the field of argon ion lasers. One can hope that besides the progress already made, the solution of the foregoing problems will lead in the nearest future to an extensive utilization of Ar^+ lasers in various branches of science and engineering.

After this review was written, two very interesting papers devoted to Ar^+ lasers were published by G. Herziger and W. Seelig[156,157]. In the first[156], an

attempt is made to develop a simplified ion-laser theory suitable for the calculation of its basic characteristics. Starting from the balance of the power fed to the discharge and consumed in it, the equations of electric conductivity with allowance for Coulomb collisions between the electrons and the ions, and the Langmuir-Tonks equation, which relates the ionization rate z with the electron temperature T_e, Herziger and Seelig obtained analytic formulas which made it possible to estimate T_e, N_e, and the true density N_a of the argon atoms in the discharge from the measured values of E and j. Further, using the theoretical values of N_e, T_e, and N_a, we obtained formulas for the pumping rate and population of the working levels of Ar^+ lasers. The formulas were obtained under the assumption that: 1) the laser levels are pumped from the ground state of the argon ion and 2) in the electron energy range from 3 to 12 eV the rate of excitation of the laser levels is proportional to the ionization rate. Herziger and Seelig did not make a detailed comparison of the calculated values of T_e and N_a with either their own data or with the published data, but the calculated values turned out to be perfectly reasonable and did not contradict the experimental results[76-80]. As to the values of N_e, according to the statement of the authors, they coincide with the experimental values[77] accurate to 10%. Nor was a comparison made between the calculated and experimental populations of the levels. A serious confirmation of the validity of the developed theory is the fact that it yields formulas previously obtained empirically, namely for the longitudinal field intensity E[66] and for the threshold current i_t[158].

The correctness of the formula obtained by the authors for the calculation of the Ar^+ laser power is convincingly confirmed by the very good agreement between the experimental dependence of the generation power at λ 4880 Å on the current, for tubes of 7 and 10 mm diameter, with the calculated dependence (see Fig. 10 of[156]).

In spite of the fact that the experimental data apparently favor the Ar^+-laser model analyzed by Herziger and Seelig, we find it necessary to call attention to a number of assumptions made by them without sufficient justification. First, the Langmuir-Tonks formula that connects the rate of ionization with the electron temperature is valid only if $\lambda_i \sim R$, whereas in the Ar^+ laser we have $\lambda_i \sim R$. Second, it is assumed that the ionization of the Ar^+ laser is effected from the ground state of the argon atom, yet one cannot exclude the possibility that ionization from the metastable states of the argon ion may play a major role and perhaps even the principal role. Third, the assumption made in[156] that the rates of ionization and excitation of the laser levels are proportional (in the electron energy range 3–12 eV) is not justified, and in fact is not true[106].

The second paper by the same authors[157] is devoted to a detailed description of the experimental investigations of ionic lasers with large-diameter tubes (7–15 mm), brief reports of which were mentioned in the review. A power of 120 W was obtained in the 4p–4s transition of Ar II in the visible region of the spectrum at a power of 1.5 W in the ultraviolet transitions of Ar III (λ 3638 and 3511 Å) and Kr III (λ 3507 Å) in the cw regime. The high inversion density (7×10^9 cm^{-3}) has made it possible to obtain superradiance of 20 W power in tubes 2 meters long at a diameter of 12 mm, on the λ 4880 and 5145 Å lines of Ar II, as a result of the amplification of the spontaneous emission and as it passed many times through the active medium. These are the main results of these two interesting papers.

[1] A. Javan, W. R. Bennett, Jr., and D. R. Herriott, Phys. Rev. Let. 6, 106 (1961).
[2] A. Schawlow, Scientific American 209, 34 (1963).
[3] W. R. Bennett, Appl. Optics Suppl. No. 1 on Optical Masers, 1962, pp. 24–62.
[4] W. R. Bennett, in: Chemical Lasers (Appl. Opt. Suppl. 2), 1965, p. 2.
[5] A. L. Bloom, Proc. IEEE 54, 1262 (1966).
[6] L. Allen and D. G. C. Jones, Advances Phys. 14, 479 (1965).
[7] A. Garscadden, in: A Survey of Phenomena in Ionized Gases, Invited Paper from the Eight International Conference on Phenomena in Ionized Gases, International Atomic Energy Agency, Vienna, 1968, p. 335.
[8] V. P. Tychinskiĭ, Usp. Fiz. Nauk 91, 389 (1967) [Sov. Phys.-Usp. 10, 131 (1967)].
[9] N. N. Sobolev and V. V. Sokovikov, ibid. 91, 425 (1967) [10, 153 (1967)].
[10] N. N. Sobolev and V. V. Sokovikov, in: The Physics of Electronics and Atomic Collisions, Invited Papers from the Fifth International Conference, 1967, p. 49 (Library of Congress Catalog Card Number 68-64013).
[11] N. N. Sobolev and V. V. Sokovikov, in: A Survey of Phenomena in Ionized Gases, Invited Paper from the Eight International Conference of Phenomena in Ionized Gases, International Atomic Energy Agency, Vienna, 1968, p. 401.
[12] Laser Focus 3 (23), 12 (1967).
[13] Laser Focus 3 (19), 21 (1967).
[14] Laser Lett. 4 (3), 2 (1967).
[15] D. de Bouard, IEEE J. Quantum Electr. QE-4 (5), 64 (1968).
[16] I. P. Segre, Proc. Natl. Electr. Conf. U.S.A., 1965, p. 48.
[17] a) R. Paananen, IEEE Spectrum 3 (6), 88 (1966), b) P. M. Armand, Ann. de radioelectr. 22, (89), 191 (1967).
[18] W. H. Mahan and J. R. Bowen, IEEE J. Quantum Electr. QE-2 (4), IX (1966).
[19] R. Hoye and J. Minton, Surg. Forum 16, 93 (1965).
[20] W. R. Bridges and A. N. Chester, Appl. Optics 4 (5), 573 (1965); IEEE J. Quantum Electr. QE-1, 66 (1965).
[21] W. R. Bennett, Jr., W. Knutson, C. N. Mercer, and J. L. Detch, Appl. Phys. Lett. 4, (10), 180 (1964).
[22] E. I. Gordon, E. F. Labuda, and W. B. Bridges, Appl. Phys. Lett. 4 (10), 178 (1964).
[23] W. B. Bridges, Appl. Phys. Lett. 4 (7), 128 (1964).
[24] G. Convert, M. Armand, and P. Martinot-Lagarde, Compt. rend. 258, 3259, 4467 (1964).
[25] W. E. Bell, Appl. Phys. Lett. 4 (2), 34 (1964).
[26] R. A. McFarlane, Appl. Opt. 3 (10), 1196 (1964).

[27] H. G. Heard and J. Peterson, Proc. IEEE 52, 1049 (1964).
[28] F. Gordon, Handb. Phys. 22, 198 (1956).
[29] E. I. Gordon and E. F. Labuda, Bell. Syst. Techn. J. 43, 1827 (1964).
[30] Electronic News 9 (450), 11 (1964).
[31] Electronics 37, 17 (1964).
[32] E. I. Gordon, E. F. Labuda, R. C. Miller, and C. E. Webb, Physics of Quantum Electronics Conference (June 28–30, 1965, San-Juan, Puerto-Rico), McGraw-Hill Book Company, p. 664.
[33] Electronics 38 (9), 17, 29 (1965).
[34] E. F. Labuda, E. I. Gordon, and R. C. Miller, IEEE J. Quantum Electr. QE-1, 273 (1965).
[35] W. E. Bell, Appl. Phys. Lett. 7, 190 (1965).
[36] W. E. Bell and A. L. Bloom, International Quantum Electronics Conference, Digest of Technical Paper (1966); IEEE J. Quantum Electr. QE-2 (4), XVII (1966), Paper 2A-3.
[37] H. Statz, F. A. Horrigan, S. H. Koozekanani, C. L. Tang, and G. F. Koster, see [32] p. 674; J. Appl. Phys. 36 (7), 2278 (1965).
[38] V. I. Donin, V. N. Klement'ev, and V. P. Chebotaev, Zh. Prikl. Spektr. 5, 368 (1966).
[39] D. A. Huchital and J. D. Rigden, IEEE J. Quantum Electr. QE-3 (9), 378 (1967).
[40] Proc. IEEE 53, 18A (1965).
[41] M. N. Demidov, N. M. Kolesnik, E. P. Ostapchenko, M. M. Raĭkher, and Yu. N. Shevchenko, Elektronnaya tekhnika ser. 3, No. 1, 103 (1967); Zh. prikl. spektr. 7, 631 (1967).
[42] I. Gorog, and F. M. Spong, Appl. Phys. Lett. 9 (1), 61 (1966).
[43] W. B. Bridges and A. S. Halsted, IEEE J. Quantum Electr. QE-2, 84 (1966).
[44] Microwaves 4 (10), 112 (1965).
[45] Electronic Design 13 (19), 16 (1965).
[46] Laser Focus 2 (13) (1966).
[47] a) H. Boersch, G. Herziger, W. Seelig, and I. Volland, Phys. Lett. 24A (12), 695 (1967). b) K. Banse, G. Herziger, G. Schäffer, and W. Selig, Phys. Lett. 27A, 682 (1968).
[48] Electronic News 10 (518), 23 (1965).
[49] Laser Focus 2 (22), 3 (1966).
[50] Laser Focus 3 (9), 38; (7), 25 (1967).
[51] R. Paananen, Appl. Phys. Lett. 9 (1), 34 (1966).
[52] G. Hernquist and J. R. Fendley, IEEE J. Quantum Electr. QE-3 (2), 66 (1967).
[53] Laser Focus 3 (21), 13 (1967).
[54] Laser Focus 4 (5), 32 (1968).
[55] Laser Focus 4 (1), 35 (1968).
[56] a) Laser Focus 3 (19), 15; (3), 22 (1967); 4 (11), 36 (1968). b) Laser Focus 4 (5), 32 (1968); 5 (1) Y19 (1969).
[57] N. A. Afonnikov, A. P. Boltaev, V. F. Kitaeva, A. E. Novik, V. P. Sasorov, and I. L. Chistyi, Svetotekhnka (Illumination Engineering) (1969).
[58] N. A. Afonnikov, A. E. Novik, and V. P. Sasorov, Enktrovak, tekhn. No. 42, 95 (1967).
[59] Electronic Design 14 (1), 38 (1966).
[60] G. Medicus and E. M. Friar, Internat. Quantum Electronics Conference, 1966, IEEE J, Quantum Electr. QF-2 (4), XX (1966).
[61] J. E. Taylor, Y. C. Kiang, F. C. Unterlitner, IEEE J. Quantum Electr. QE-2 (4), XIX (1966), Paper 3B-2.
[62] J. P. Goldsborough, E. B. Hodges, and W. E. Bell, Appl. Phys. Lett. 8 (6), 137 (1966).
[63] Laser Focus 3 (1), 25 (1967).
[64] C. B. Zarowin and C. K. Williams, Appl. Phys. Lett. 11 (2), 47 (1967).
[65] J. P. Goldsborough, Appl. Phys. Lett 8 (9), 218 (1966).
[66] A. N. Chester, Phys. Rev. 169 (1), 172, 184 (1968); Gas Pumping in Discharge Tubes, Bell Telephone Laboratories, New Jersey. Preprint (1967).
[67] P. K. Cheo and H. G. Cooper, Appl. Phys. Lett. 6, 177 (1965).
[68] N. G. Preobrazhenskii, Opt. spektrosk. 25, 317 (1968).
[69] I. Gorog and F. W. Spong, RCA Rev. 28 (1), 38 (1967).
[70] M. Birnbaum, Appl. Phys. Lett. 12 (3), 86 (1968).
[71] S. A. Ahmed and T. J. Faith, Jr., Proc. IEEE 54, (10), 1470 (1966).
[72] P. L. Rubin, Zh. Tekh. Fiz. 38, 489 (1968) [Sov. Phys.-Tech. Phys. 13, 361 (1968)].
[73] B. A. See, W. Garwoli, and J. L. Hughes, IEEE J. Quantum Electr. QE-3 (4), 169 (1967).
[74] G. de Mars, M. Seiden and F. Horrigan, IEEE J. Quantum Electr. QE-4 (5), 42; (10), 631 (1968).
[75] S. E. Frish and Yu. M. Kagan, Zh. Eksp. Teor. Fiz. 11, 286 (1941), 12, 342 (1942), 17, 577 (1947), 18 (519 (1948); Izv. AN SSSR ser. fiz. 12, 358 (1958); V. M. Zakharova and Yu. M. Kagan, Opt. Spektrosk. 1, 627 (1957).
[76] V. F. Kitaeva, Yu. I. Osipov, and N. N. Sobolev, Dokl. Akad. Nauk SSSR 172, 317 (1967) [Sov. Phys.-Dokl. 12, 55 (1967)].
[77] V. F. Kitaeva, Yu. I. Osipov, and N. N. Sobolev, IEEE J. Quantum. Electr. QE-2 (9), 635 (1966).
[78] V. F. Kitaeva, Yu. I. Osipov, and N. N. Sobolev, ZhETF Pis. Red. 4, 213 (1966) [JETP Lett. 4, 146 (1966)].
[79] V. F. Kitaeva, Yu. N. Osipov, N. N. Sobolev, and P. L. Rubin, Zh. Tekh. Fiz. 37, 1173 (1967) [Sov. Phys.-Tech. Phys. 12, 850 (1967)].
[80] V. F. Kitaeva, Yu. I. Osipov, L. Ja. Ostrovskaya, and N. N. Sobolev, Phenomena in Ionized Gases, Contributed Papers on International Conference, Vienna, 1967, p. 257.
[81] A. E. Ballik, W. R. Bennett, Jr., and G. N. Mercer, Appl. Phys. Lett. 8 (8), 214 (1966).
[82] A. A. Boguslovskiĭ, T. T. Gur'ev, D. N. Didrikil', V. A. Novikova, V. V. Kyun, A. F. Stepanov, and V. A. Stepanov, Elektron. tekhn. ser. 3, No. 1, 8 (1967)].
[83] E. F. Labuda, C. E. Webb, R. C. Miller, and E. I. Gordon, Bull. Amer. Phys. Soc. 11, 497 (1966).
[84] G. N. Mercer, V. P. Chebotayev, W. R. Bennett, Appl. Phys. Lett. 10, 177 (1967).
[85] W. R. Bennett, Jr., A. E. Ballik, and G. N. Mercer, Phys. Rev. Lett. 16 (14), 603 (1966).
[86] R. J. Carbone and M. M. Litvak, Bull. Amer. Phys. Soc. 11 (1), 128 (1966).
[87] R. C. Miller, E. F. Labuda, and C. E. Webb, Bell. Syst. Techn. J. 46 (1), 281 (1967).
[88] C. E. Webb, 19th Annual Gaseous Electronics

Conference (Atlanta, Georgia, October 1966), p. 14.
[89]A. Caruso and A. Cavaliere, Brit. J. Appl. Phys. 15, 1021 (1964).
[90]B. N. Klyarfel'd, Trudy VEI 41, 165 (1940).
[91]P. T. Smith, Phys. Rev. 36, 1293 (1930).
[92]Yu. M. Kagan and V. I. Perel', Opt. spektrosk. 2, 298 (1957); 4, 3 (1958).
[93]A. von Engel, Ionized Gases, Oxford, 1955.
[94]V. N. Kolesnikov, Trudy FIAN 30, 66 (1964).
[95]S. D. Gvozdover, Zh. Eksp. Teor. Fiz. 7, 867 (1937).
[96]J. R. Forrest and R. H. Franklin, Brit. J. Appl. Phys. 17, 1061, 1569 (1966).
[97]S. M. Borisova, E. F. Ishchenko, V. M. Ladygin, M. A. Molchashkin, E. F. Nasedkin, G. S. Ramazanova, Radiotekhn. i élektron. 12, 562 (1967).
[98]V. F. Kitaeva, Yu. I. Osipov, P. L. Rubin, and N. N. Sobolev, On Oscillation Mechanism in cw-Ion Argon Laser, Preprint (1968); IEEE J. Quantum Electr. 5 (2), 72 (1969).
[99]H. Marantz, Thesis (Cornell University, Ithaca, N. Y., 1968).
[100]H. F. Berg and W. Ervens, Zs. Phys. 206 (2), 184 (1967).
[101]H. N. Olsen, J. Quantum Spectr. Radiat. Transfer 3, 59 (1963).
[102]F. A. Horrigan, S. H. Koozekanani, and R. A. Paananen, Appl. Phys. Lett. 6 (3), 41 (1965).
[103]W. R. Bennett, Jr., P. J. Kindlmann, C. N. Mercer, and J. Sunderland, Appl. Phys. Lett. 5, 158 (1964).
[104]J. Bakos, J. Szigeti, L. Varga, Phys. Lett. 20, 503 (1966).
[105]B. A. Tozer and J. D. Craggs, J. Electr. Control 8, 107 (1960).
[106]I. L. Beĭgman, L. A. Vaĭnshteĭn, P. L. Rubin and N. N. Sobolev, ZhETF Pis. Red. 6, 919 (1967) [JETP Lett. 6, 343 (1967)].
[107]L. A. Vaĭnshteĭn, Opt. spektrosk. 11, 301 (1961).
[108]L. M. Biberman, Zh. Eksp. Teor. Fiz. 17, 416 (1947); Dokl. Akad.Nauk SSSR 49, 659 (1948).
[109]T. Holstein, Phys. Rev. 72, 1212 (1947); 83, 1159 (1951).
[110]R. I. Rudko and C. L. Tang, J. Appl. Phys. 38, 4731 (1967).
[111]W. R. Bennett et al., Phys. Rev. Lett. 17, 987 (1966).
[112]R. J. Bickerton and A. von. Engle, Proc. Phys. Soc. 69B, 468 (1956).
[113]V. E. Golant, M. V. Krivosheev, and V. E. Privalov, Zh. Tekh. Fiz. 34, 953 (1964) [Sov. Phys.-Tech. Phys. 9, 737 (1964)].
[114]F. A. Korolev, A. I. Odintsov, V. V. Lebedeva, S. S. Ptkova, and D. M. Mashtakov, Zh. Prikl. Spektr. 11, 351 (1969).
[115]W. W. Rigrod and T. J. Bridges, IEEE J. Quantum Electr. QE-1 (7), 298, 303 (1965).
[116]V. V. Lebedeva, A. I. Odintsov, and V. M. Salimov, Zh. Tekh. Fiz. 38, 1373 (1968) [Sov. Phys.-Tech. Phys. 13, 1122 (1969)].
[117]R. E. McClure, Appl. Phys. Lett.77 (6), 148 (1965).
[118]P. W. Smith, IEEE J. Quantum Electr. QE-3 (11), 627 (1967).
[119]R. L. Fork and M. A. Pollack, Phys. Rev. 139 (5a), 1408 (1965).
[120]M. S. Borisova and A. M. Pyndyk, Radiotekhn. i élektron. 13, 754 (1968).
[121]M. Bass, G. de Mars, and H. Statz, Appl. Phys. Lett. 12 (1), 17 (1968).
[122]C. L. Tang and H. Statz, J. Appl. Phys. 39 (1), 31 (1968).
[123]a) O. L. Gaddy and E. M. Schaefer, Appl. Phys. Lett. 9 (8), 281 (1966). b) I. Gorog and F. W. Spong, IEEE J. Quantum Electr. QE-3 (12), 691 (1967).
[124]A. L. Bloom, Appl. Phys. Lett. 2, 101 (1963).
[125]M. A. Halegger, T. J. Harris, and E. Max, IBM J. Res. and Developm. 10 (4), 346 (1966).
[126]K. M. Baird, D. S. Smith, G. R. Hanes, and S. Trunekane, Appl. Opt. 4 (5), 569 (1965).
[127]P. Zory, J. Appl. Phys. 37,(9), 3643 (1966).
[128]W. R. Bennett, Phys. Rev. 126, 580 (1962).
[129]P. W. Smith, IEEE J. Quantum Electr. 1 (8), 343 (1965); 2 (9), 666 (1966).
[130]P. Zory, IEEE J. Quantum Electr. QE-3 (10), 390 (1967).
[131]A. I. Odintsov, V. V. Lebedeva, G. V. Abrosimov, Radiotekhn. i élektron. 31, 746 (1968).
[132]I. Gorog and F. W. Spong, Laser Focus 4 (1), 21 (1968).
[133]D. C. Sinclair, JOSA 56, 12, 1727 (1966).
[134]a) V. P. Belyaev, V. A. Burmakin, A. N. Evtyunin, F. A. Korolev, V. V. Lebedeva, and A. I. Odintsov, Paper at Conf. on Quantum Electronics, Erevan, October 1967. b) D. C. Sinclair, Appl. Phys. Lett. 13, 98 (1968).
[135]W. W. Rigrod and A. M. Johnson, IEEE J. Quantum Electr. QE-3 (11), 644 (1967).
[136]L. M. Osterink and R. Targ, Appl. Phys. Lett. 10 (4), 115 (1967).
[137]G. A. Massey, M. K. Oshman, and R. Targ, Appl. Phys. Lett. 6, 10 (1965).
[138]S. E. Harris and O. P. McDuff, Appl. Phys. Lett. 5 (10), 205 (1964).
[139]S. E. Harris, Proc. IEEE 54 (10), 140 (1966).
[140]S. E. Harris, M. K. Oshman, B. J. McMurtry, and E. O. Ammann, Appl. Phys. Lett. 7, 184 (1965).
[141]R. Targ, L. M. Osterink, and J. M. French, Proc. IEEE 55, 7 (1967).
[142]Yu. V. Troitskiĭ and N. D. Goldina, ZhETF Pis. Red. 7, 49 (1968) [JETP Lett. 7, 36 (1968)]; Opt. spektrosk. 25, 462 (1968).
[143]J. M. Forsyth, Appl. Phys. Lett. 11, (12), 391 (1967).
[144]W. E. Lamb, Phys. Rev. 134A (6), 1429 (1964).
[145]A. D. White, E. I. Gordon and J. D. Rigden, Appl. Phys. Lett. 2 (5), 91 (1963).
[146]W. W. Rigrod, J. Appl. Phys. 34, 2602 (1963).
[147]E. I. Gordon, A. D. White and J. D. Rigden, Symposium on Optical Masers, N. Y., 1963, p. 309.
[148]W. W. Rigrod, J. Appl. Phys. 36 (8), 2487 (1965).
[149]A. G. Velichko, Zh. Prikl. Spetkrosk. 4, 30 (1966).
[150]A. Szöke and A. Javan, Phys. Rev. 145 (1), 137 (1966).
[151]A. G. Fox and T. Li, IEEE J. Quantum Electr. QE-2 (12), 774 (1966).
[152]A. I. Odintsov, V. V. Lebedeva, and I. V. Shafranovskaya, Zh. Tekh. Fiz. 39, 107 (1969) [Sov. Phys.-Tech. Phys. 14, 000 (1969)].
[153]A. I. Odintsov, V. V. Lebedeva, and Yu. V.

Kuratov, Zh. Prikl. Spektrosk. 6, 598 (1967).
[154] A. I. Odintsov, V. V. Lebedeva, and V. A. Sautkin, ibid. 7, 754 (1967).
[155] C. E. Webb, R. C. Miller, and C. L. Tang, Internat. Quant. Electr. Conference, Miami, 1968, IEEE J. Quantum Electr. QE-4 (5), 46 (1968), Paper 12L-6.
[156] G. Herziger and W. Seelig, Zs. Phys. 215, 437 (1968).
[157] G. Herziger and W. Seelig, Zs. Phys. 219, 5 (1969).
[158] E. F. Labuda and A. M. Johnson, IEEE J. Quantum Electr. QE-2 (10), 700 (1966).
[159] P. W. Smith, IEEE. J. Quantum Electr. QE-2 (3), 62 (1966).
[160] H. Statz, G. A. de Mars and C. L. Tang, Appl. Phys. Lett. 14 (4), 125 (1969).

REFERENCES ADDED IN PROOF

Chapter III:

[161] Laser Focus 5 (9), 11 (1969).
[162] W. H. McMahan, Appl. Phys. Lett. 12 (11), 383 (1968).
[163] A. Ferrario and A. Sona, IEEE J. Quantum Electr. QE-5 (2), 124 (1969).

Chapter V:

[164] H. C. Koons, Giorgio Fiocco, J. Appl. Phys. 39 (7), 3389 (1968).
[165] M. Hudis, K. Chung, and D. J. Rose, J. Appl. Phys. 39 (7), 3297 (1968).
[166] S. A. Ahmed, T. J. Faith, and G. W. Hoffman, Proc. IEEE 55 (5), 691 (1967).
[167] I. D. Kon'kov, R. E. Rovinskiĭ, A. G. Rozanov, and N. V. Cheburkin, Radiotekhn. i élektron. 13, 2280 (1968).
[168] W. R. Benett, Jr., V. P. Chebotayev, and J. W. Knutson, Jr., Phys. Rev. Lett. 18 (17), 688 (1967).
[169] J. Blandin, S. Brechot-Sahal, and J. Chapelle, A. Sy, Phys. Lett. 26A (10), 487 (1968).
[170] C. E. Webb, J. Appl. Phys. 39 (12), 5441 (1968).

Chapter VI:

[171] J. M. Hammer and C. P. Wen, J. Chem. Phys. 46 (4) 1225 (1967).
[172] F. A. Korolev, V. V. Lebedeva, A. I. Odintsov, and V. M. Salikov, Radiotekhn. i élektron. 14, 1519 (1969).
[173] S. C. Lin and C. C. Chen, Bull. Am. Phys. Soc. 14 (8), 839 (1969).
[174] T. T. Gur'ev, V. V. Kyun, G. I. Mal'kova, E. P. Ostapchenko, and V. A. Stepanov, Elektron. tekhn. ser. 3, No. 2, 3 (1969).
[175] G. R. Levinson, V. F. Papulevskiĭ, and V. P. Tychinskiĭ, Radiotekhn. i élektron. 13, 663 (1968).
[176] M. S. Borisova, E. F. Ishchenko, M. V. Ladygin, M. A. Molchashkin, E. F. Nasedkin, and G. S. Ramazanova, ibid. 12, 565 (1967).
[177] S. Koozekanani, Appl. Phys. Lett. 11 (3), 107 (1967).
[178] H. Marantz, R. J. Rudko, and C. L. Tang, Appl. Phys. Lett. 9 (11), 409 (1966).
[179] R. J. Rudko and C. L. Tang, Appl. Phys. Lett. 9 (1), 41 (1966).
[180] T. H. E. Cotrell, IEEE J. Quantum Electr. QE-4 (7), 435 (1968).

Chapter VIII:

[181] D. C. Jones, M. D. Sayers, and L. Allen, J. Phys. A. (Gen. Phys.), ser. 2, 2 (1), 95 (1969).

Chapter IX:

[182] Y. I. Donin, Yu. V. Troitskiĭ, and N. D. Goldina, Opt. spektrosk. 26, 118 (1969).
[183] Yu. V. Troitskiĭ, Radiotekhn. i élektron. 14, 1641 (1969).
[184] P. W. Smith, M. V. Schneider, and H. G. Danielmeyer, Bell. Syst. Techn. J. 48 (5), 1405 (1969).
[185] H. Merkelo, R. H. Wright, E. P. Bialecke, and J. P. Kaplafka, Appl. Phys. Lett. 12, (10), 337 (1968).

Translated by J. G. Adashko